

A Large, Uniform Sample of X-ray Emitting AGN: Selection Approach and an Initial Catalog from the ROSAT All-Sky and Sloan Digital Sky Surveys

Scott F. Anderson¹, Wolfgang Voges², Bruce Margon³, Joachim Trümper², Marcel A. Agüeros¹, Thomas Boller², Matthew J. Collinge⁴, L. Homer¹, Gregory Stinson¹, Michael A. Strauss⁴, James Annis⁵, Percy Gomez⁶, Patrick B. Hall^{4,7}, Robert C. Nichol⁶, Gordon T. Richards⁴, Donald P. Schneider⁸, Daniel E. Vanden Berk⁹, Xiaohui Fan¹⁰, Željko Ivezić⁴, Jeffrey A. Munn¹¹, Heidi Jo Newberg¹², Michael W. Richmond¹³, David H. Weinberg¹⁴, Brian Yanny⁵, Neta A. Bahcall⁴, J. Brinkmann¹⁵, Masataka Fukugita¹⁶, Donald G. York¹⁷

email addresses: anderson@astro.washington.edu, wvoges@mpe.mpg.de, margon@stsci.edu

ABSTRACT

Many open questions in X-ray astronomy are limited by the relatively small number of objects in uniform optically-identified and observed samples, especially when rare subclasses are considered, or when subsets are isolated to search for evolution or correlations between wavebands. We describe initial results of a new program aimed to ultimately yield $\sim 10^4$ fully characterized X-ray source identifications—a sample

¹University of Washington, Department of Astronomy, Box 351580, Seattle, WA 98195.

²Max Planck-Institute für extraterrestrische Physik, Geissenbachstr. 1, D-85741 Garching, Germany.

³Space Science Telescope Institute, 3700 San Martin Drive, Baltimore, MD, 21218.

⁴Princeton University Observatory, Princeton, NJ 08544.

⁵Fermi National Accelerator Laboratory, P.O. Box 500, Batavia, IL 60510.

⁶Dept. of Physics, Carnegie Mellon University, 5000 Forbes Ave., Pittsburgh, PA 15232.

⁷Departamento de Astronomía y Astrofísica, Facultad de Física, Pontificia Universidad Católica de Chile, Casilla 306, Santiago 22, Chile

⁸Department of Astronomy and Astrophysics, The Pennsylvania State University, University Park, PA 16802.

⁹Dept. of Physics and Astronomy, University of Pittsburgh, Pittsburgh, PA 15260.

¹⁰Steward Observatory, The University of Arizona, Tucson, AZ 85732.

¹¹US Naval Observatory, Flagstaff Station, P.O. Box 1149, Flagstaff, AZ 86002-1149.

¹²Dept. of Physics, Applied Physics and Astronomy, Rensselaer Polytechnic Institute, Troy NY 12180.

¹³Department of Physics, Rochester Institute of Technology, Rochester, NY 14623-5603.

¹⁴Department of Astronomy, Ohio State University, Columbus, OH 43210.

¹⁵Apache Point Observatory, P.O. Box 59, Sunspot, NM 88349-0059.

¹⁶Institute for Cosmic Ray Research, University of Tokyo, Midori, Tanashi, Tokyo 188-8588, Japan

¹⁷Astronomy and Astrophysics Center, University of Chicago, 5640 South Ellis Avenue, Chicago, IL 60637.

about an order of magnitude larger than earlier efforts. The technique is detailed, and employs X-ray data from the ROSAT All-Sky Survey (RASS), and optical imaging and spectroscopic follow-up from the Sloan Digital Sky Survey (SDSS); these two surveys prove to be serendipitously very well matched in sensitivity. As part of the SDSS software pipelines, optical objects in the SDSS photometric catalogs are automatically positionally cross-correlated with RASS X-ray sources. Then priorities for follow-on SDSS optical spectra of candidate counterparts are automatically assigned using an algorithm based on the known ratios of f_x/f_{opt} for various classes of X-ray emitters at typical RASS fluxes of $\sim 10^{-13}$ erg cm $^{-2}$ s $^{-1}$. SDSS photometric parameters for optical morphology, magnitude, colors, plus FIRST radio information, serve as proxies for object class.

Initial application of this approach to RASS/SDSS data from 1400 deg 2 of sky provides a catalog of more than 1200 spectroscopically confirmed quasars and other AGN that are probable RASS identifications. Most of these are new identifications, and only a few percent of the AGN counterparts are likely to be random superpositions. The magnitude and redshift ranges of the counterparts are very broad, extending over $15 < m < 21$ and $0.03 < z < 3.6$, respectively. Although most identifications are quasars and Seyfert 1s, a variety of other AGN subclasses are also sampled. Substantial numbers of rare AGN types are found, including more than 130 narrow-line Seyfert 1s and 45 BL Lac candidates. These early results already provide a very sizeable set of source identifications, demonstrate utility of the sample in multi-waveband investigations, and show the capability of the joint RASS/SDSS approach to efficiently proceed towards the largest homogeneously selected/observed sample of X-ray emitting quasars and other kinds of AGN.

Subject headings: catalogs — surveys — quasars: general — quasars: individual — X-rays

1. Introduction

Although extrasolar X-ray sources were first observed four decades ago (Giacconi et al. 1962), the first all-sky *imaging* X-ray survey has only recently been achieved. The ROSAT All-Sky Survey (hereafter RASS; Voges et al. 1999, 2000) covers the entire celestial sphere in the 0.1 – 2.4 keV range with the Position Sensitive Proportional Counter (PSPC; Pfeiffermann et al. 1988) to a typical limiting sensitivity of $\sim 10^{-13}$ erg cm $^{-2}$ s $^{-1}$, although due to the scanning protocol, the exposure times and thus sensitivity limits vary markedly from the ecliptic pole to equator. Depending on the level of statistical significance discussed, 10^4 – 10^5 X-ray sources are contained in the RASS Bright and Faint Source Catalogs, with more than 124,000 sources in the catalog versions considered here. Positional accuracies derivable for the sources vary with count

rate, but moderately well-exposed sources typically have a positional uncertainty of $\sim 10 - 30''$. Many important inferences can and have been made from RASS data based directly on the X-ray observations alone, with minimal need for new correlative observations at other wavelengths. For example, the RASS point source catalogs provide an exceptional measure of a portion of the X-ray log N/log S diagram (e.g., Voges et al. 1999).

However, the scale of the effort involved in identifying a large fraction of the abundant RASS sources, especially those in the Faint Source Catalog, poses an unusual analysis problem. From ROSAT and also previous generations of X-ray observatories, especially the extensive observations of the *Einstein Observatory* (e.g., Gioia et al. 1984), such X-ray source counterparts are known to include a highly heterogeneous mix of objects, ranging from nearby M dwarfs to distant quasars. In many cases, the X-ray data taken alone cannot unambiguously determine whether an X-ray source is Galactic or extragalactic, much less finer distinctions about its nature. It has thus long been realized that identification of optical counterparts is an essential companion study to large X-ray surveys.

The most complete optical identification effort attempted on *Einstein* X-ray data was that of the Extended Medium Sensitivity Survey (EMSS; e.g., Stocke et al. 1991). The comparison with RASS is not inappropriate, as although *Einstein* surveyed $< 10\%$ of the celestial sphere, the flux levels and positional accuracy of source determinations from the *Einstein* Imaging Proportional Counter detector were not greatly dissimilar to the ROSAT PSPC (though, for example, the latter provides better positional information). Optical identification of sources in the EMSS have been made in an exceptionally ambitious, decade-long program (e.g., Stocke et al. 1991 and references therein), with confirming optical spectra taken one at a time, using a heterogeneous collection of telescopes and detectors, the only plausible facilities available at that time. The EMSS yielded an impressive ~ 800 optical counterparts, including normal stellar coronae, pre-main-sequence stars, interacting binaries, supernova remnants, nearby galaxies, clusters of galaxies, and, especially, active galactic nuclei (AGN) of a broad range of luminosities. Quasars/AGN are the predominant class in the EMSS, accounting for more than 400 of the *Einstein* identifications.

In a similar effort devoted to ROSAT data, there have been successful optical identification programs conducted, or still in progress, on bright subsets of the RASS, or complete subsets over small regions of sky, by a large collaboration (Fischer et al. 1998, Zickgraf et al. 1998, Schwobe et al. 2000). The goal is again $\sim 10^3$ optical identifications. In addition, a remarkably resourceful effort using the Hamburg objective prism plates (Bade et al. 1998a, Zickgraf et al. 2003) has resulted in the tabulation of candidate identifications for a significant number of the brightest RASS sources. Typically AGN are inferred as the correct identification if an object with $B < 18.5$ has a blue continuum color over the 2000 \AA of plate coverage; often emission lines are not detectable. However even for this brighter subset, accurate redshifts, magnitudes, optical continuum slopes, and emission line identifications, intensities, and equivalent widths are largely unavailable.

Although the $\sim 10^3$ total identifications from $\sim 10^3 \text{ deg}^2$ of sky provided by the EMSS (and similar later ROSAT surveys) is an extremely respectable number, there remain scientific problems where the size of an identified *subclass* of X-ray emitter of interest is uncomfortably small. Notable examples include studies of the more rare subclasses of AGN, such as narrow-line Seyfert 1s (hereafter, NLS1s) and BL Lacs. For example, among the large sample of more than 400 AGN from the EMSS, only about ~ 40 BL Lacs were found; and yet, even this small subsample suggested remarkable “negative evolution” (e.g., Morris et al. 1991) that demands further study. If such rare subclasses of AGN evolve in their properties with redshift, and/or exhibit complex dependencies of X-ray luminosity with optical and/or radio luminosity, as more typical quasars are known to do (e.g., Avni & Tananbaum 1986; Wilkes et al. 1994; Avni, Worrall, & Morgan 1995), then an already small subsample must be further subdivided into yet smaller bins for analysis, leaving literally a handful of objects per bin. Another, less obvious, example is that although modest- to high-redshift quasars are not usually thought of as “rare”, X-ray selection at the *Einstein* and RASS flux levels strongly favors the discovery of nearby and low luminosity AGN; in fact, the entire EMSS sample of > 400 AGN includes only a small handful of X-ray emitting quasars with $z > 2$, thus limiting its utility for studies of the quasar X-ray luminosity function at moderate- to high-redshift.

In order to effectively build and expand upon such earlier large scale counterpart identification programs, any new effort (at comparable X-ray depth) must survey substantially in excess of the $\sim 10^3 \text{ deg}^2$ covered by the EMSS, and must ultimately provide a sample numbering substantially in excess of $\sim 10^3$ optical identifications, obtained in uniform fashion. Moreover, if many more than 10^3 counterparts are to be newly found on a reasonable timescale, more efficient optical identification techniques than previously available must be used. The requisite large X-ray sample is now available via the RASS Bright and Faint Source Catalogs; the more efficient optical identification and analysis technique is provided by the Sloan Digital Sky Survey (SDSS, e.g., York et al. 2000, Stoughton et al. 2002, Abazajian et al. 2003).

In this paper we describe initial results of a program that exploits the unique combined capabilities of the ROSAT and Sloan Surveys to eventually obtain a sample of $\sim 10^4$ X-ray sources, which are not only optically identified, but which also have high quality and uniform data in the X-ray from RASS and in the optical (photometry and spectroscopy) from SDSS. Our emphasis in this initial paper is on high-confidence RASS/SDSS optical identifications of quasars and other AGN. In section 2 we provide a brief description of relevant aspects of the SDSS data, and the fortuitous match in sensitivity to the RASS. In section 3, we detail the technique used to select and confirm candidate counterparts from the SDSS data. In section 4, we present results from this RASS/SDSS program for 1400 deg^2 of sky, providing an initial catalog (optical photometry and spectroscopy, as well X-ray properties) of more than 1200 likely AGN identifications for RASS X-ray sources, including 45 BL Lac candidates. In section 5, we discuss a few additional AGN subcategories and objects of special interest, including NLS1s. Section 6 provides an overview of the ensemble properties of the initial sample, especially as they pertain to the reliability of the

identifications. Section 7 provides an illustrative example of optical/X-ray correlation studies that may be enabled by the sample. A very brief summary is provided in Section 8.

2. The Excellent Match Between SDSS Optical and RASS X-ray Surveys

The Sloan Digital Sky Survey (SDSS) is a multi-institutional project to create an optical digital imaging and spectroscopic data bank of a large portion of the celestial sphere, mainly in a region approaching $\sim 10^4 \text{ deg}^2$ centered on the north Galactic polar cap. A recent overview of the project has been given by York et al. (2000), and a comprehensive technical description of the large subset of the software pipelines and data released earlier to the public is available in Stoughton et al. (2002). The optical data are obtained by a special purpose 2.5m telescope, located at Apache Point Observatory, New Mexico, built and optimized solely for this project. It is equipped with a unique mosaic camera (Gunn et al. 1998) which operates in TDI (Time Delay and Integrate) mode that can image $\sim 10^2 \text{ deg}^2$ in 5 colors in a single night, as well as a multifiber spectrograph which obtains the spectra of 640 objects within a 7 deg^2 field simultaneously. The resulting photometric atlas is in 5 specially-chosen colors u, g, r, i, z (Fukugita et al. 1996, Hogg et al. 2001, Smith et al. 2002) from ~ 3600 to $10,000 \text{ \AA}$, covering the entire survey area to a limiting magnitude of $r \sim 22-23$, on $0.4''$ pixels. This database is automatically analyzed to catalog the photometric and astrometric properties of several hundred million stars and galaxies, as well as a million quasars. The imaging database is used to autonomously and homogeneously select objects for the SDSS spectroscopic survey, which will ultimately include moderate resolution ($\lambda/\Delta\lambda \sim 1800$) spectrophotometry covering a broad ($3800-9200\text{\AA}$) wavelength regime for 10^6 galaxies, 10^5 quasars, and 10^5 unusual stars.

The RASS and SDSS are extremely well-matched to each other via a variety of fortunate coincidences. For example, the SDSS survey area is also the region of greatest RASS X-ray sensitivity, because it lies primarily at high ecliptic latitude (and thus long RASS exposure times) and also high Galactic latitude (and thus regions of low interstellar photoelectric opacity, an important effect in the soft ROSAT energy band).

Perhaps most important, the limiting X-ray flux of RASS is such that, given the known range of f_x/f_{opt} for most common classes of sources, both Galactic and extragalactic, even the optically faintest counterparts of typical RASS sources are accessible to both the SDSS photometric and spectroscopic surveys. For example, although there is considerable dispersion, the most X-ray luminous (relative to optical) normal stars, normal galaxies, quasars, and BL Lacs are known to have $\log (f_x/f_{opt})$ of about -1, -0.25, 1.0, and 1.5 respectively (*e.g.*, Stocke et al. 1991). At the limiting RASS X-ray flux quoted above, this implies that even unusually faint optical counterparts in each of these classes will have magnitudes brighter than $m \sim 15, 17, 20, \text{ and } 21$, respectively. Thus the SDSS imaging survey will obtain highly accurate colors and magnitudes for the vast majority of RASS counterparts, and even the spectroscopic portion of SDSS, where the ~ 45 minute exposure times are set primarily to provide acceptable signal for the galaxies

in the large scale structure survey, will yield excellent quality spectra for the large majority of counterparts, permitting confident identifications and in-depth subsequent analyses.

Additionally, the full RASS/SDSS area is also covered by the NVSS and/or FIRST 20 cm radio surveys (Condon *et al.* 1998; Becker, White & Helfand 1995). Thus radio information is also available for virtually *every* interesting RASS/SDSS object.

The final part of the good match between RASS and SDSS is a consequence of the modest surface density of RASS sources on the sky—commonly, a few sources per square degree. A typical SDSS spectroscopic field of about 7 deg^2 thus has $\sim 10^1$ RASS sources, and therefore $\sim 10^4$ RASS sources in the ultimate SDSS sky coverage can be targeted for at least one spectroscopic observation, while only diverting 1% of the fibers from other SDSS scientific programs.

3. Autonomous Selection of Candidate Optical Counterparts for SDSS Spectra

As noted above, a subset of objects of special interest in the SDSS imaging are slated for follow-up SDSS spectroscopy; objects are selected from the imaging database via various algorithms that comprise the SDSS “target selection” pipeline software (Stoughton *et al.* 2002). As part of that target selection pipeline, we have implemented algorithms aimed to specifically select candidate ROSAT counterparts for automated SDSS spectra. Optical objects in the SDSS photometric catalogs are automatically cross-correlated with objects in the RASS X-ray catalogs (Bright and Faint Source). Those SDSS optical objects within $1'$ of the X-ray source positions are initially flagged (with a database flag ‘rosatMatch’ having value >0) as potential positional matches in the imaging catalogs and considered further, though not all will receive follow-on SDSS spectra as we detail below.

As our eventual goal is the optical identification of $\sim 10^4$ RASS X-ray sources (a sample approximately an order of magnitude larger than previous efforts), we emphasize SDSS spectroscopic follow-up of that subset of the cataloged RASS sources which have the highest X-ray detection likelihoods (a maximum likelihood measure of the RASS X-ray source significance; see Voges *et al.* 1999). In the RASS/SDSS target selection algorithm, the minimum X-ray detection likelihood parameter is currently set to ≥ 10 ; this cut, imposed on the RASS catalog, yields the desired highest-significance $\sim 10^4$ X-ray sources in the ultimate joint RASS/SDSS sky coverage.

While it would be optimal to take optical spectra of all objects within each such RASS error circle, this is not feasible for several reasons in practice. First, the minimum allowed spacing between SDSS spectroscopic fibers is $55''$, and most error circles will be sampled spectroscopically on only a single occasion during the course of the entire SDSS survey. Second, the SDSS imaging data extend to beyond $m \sim 22$, and therefore the faintest optical images detected are significantly fainter than the SDSS spectroscopic limits. A compromise is made to generally aim for taking an SDSS spectrum of a single optical object in each RASS error circle (with X-ray maximum-likelihood value ≥ 10) covered by SDSS. The optical object chosen for SDSS

spectroscopy in each RASS circle must also be brighter than $m < 20.5$ (more specifically, g , r , or $i < 20.5$); this is the magnitude limit for good quality SDSS spectra of emission line objects in the typical 45 minute spectroscopic exposure times. There is also a bright limit of $m > 15$, needed to avoid spectroscopic cross-talk between nearby multi-object fibers.

An additional complication is that, for technical reasons, photometric measures for all SDSS optical objects within each RASS circle may not generally be *intercompared* to one another at the stage when algorithmically selecting targets for SDSS optical fiber spectroscopy.¹⁸ Thus, rather than using the SDSS multicolor imaging data to select the “best” candidate optical counterpart in each RASS circle for a spectrum, we instead (at the target selection stage) must independently assess the quality of each optical object in the RASS circle on an absolute scale, without knowledge of (or direct comparison to) any other positionally consistent optical objects.

Our approach is thus to assign every SDSS optical object (imaged at the time of “target selection”) within the RASS circle to a broad priority bin grade (A,B,C,D) for optical spectroscopy. These priority bins are based on typical ratios of X-ray to optical flux for various classes of known X-ray emitters, at a typical limiting RASS X-ray flux of a few times 10^{-13} erg/sec/cm², and are used to gauge identification likelihoods and hence assign spectroscopic priorities for SDSS candidate optical counterparts. SDSS optical magnitudes, colors and morphology parameters, as well as FIRST radio data, serve as proxies at this stage for the likely object class.

Among the various possible priority bins for ROSAT counterpart identifications, we have chosen objects having a triple positional coincidence between a RASS X-ray source, an SDSS optical object, and a FIRST radio source, for highest priority for SDSS optical spectra; the SDSS object and FIRST source must match to within 2” (which we note may miss some radio sources with complex morphology). As mentioned above, virtually 100% of the SDSS area will also be covered by the FIRST 20 cm radio survey, although the relevant FIRST catalogs may not always have been available when the SDSS target selection software was actually run. The cross-correlation with FIRST catalogs (also done automatically) is mainly intended to ensure sensitivity to BL Lacs and other X-ray/radio-emitting quasars, but this algorithm also finds, for example, radio galaxies (isolated and in clusters), etc. These highest-priority triple-waveband RASS/SDSS/FIRST coincidences are flagged as ‘ROSAT_A’ objects by the target selection pipeline software, and indicated as such in the SDSS database.

Objects in RASS error circles with unusual SDSS colors indicative of AGN and quasars (but lacking FIRST detections) are given next priority for SDSS optical spectra. Simple UV-excess selection $u - g < 0.6$ built into the RASS/SDSS target selection module, as well as far more sophisticated approaches (Richards et al. 2002; Newberg & Yanny 1997) looking for outliers in the full SDSS 4-dimensional color space, are consulted in assigning objects to this potential AGN

¹⁸For example, in an extreme case it could even be that early SDSS optical imaging covers only some portion of a given X-ray error circle, while optical imaging coverage of the remainder of the X-ray error circle will not be completed until very late in the survey.

class. All such second-highest priority potential spectroscopic targets are flagged as ‘ROSAT_B’ by the target selection algorithm module. In fact, more than 90% of the confirmed RASS/SDSS quasars/AGN are selectable by the simple UV-excess criterion (see Figure 1); this is not surprising, as X-ray selection at the RASS flux limits has long been known to favor low-luminosity quasars and related AGN at low-redshift (e.g., Margon, Chanan, & Downes 1982). These color-outlier selections (especially because of the sensitivity to UV-excess) also sometimes yield identifications which, upon examination of the SDSS spectra, turn out to be X-ray emitting cataclysmic variables, white dwarfs, etc. (The latter classes are the topics of other SDSS papers).

The third broad priority bin includes a varied set of somewhat less likely or less interesting, but still plausible, identifications including: bright stars and galaxies (currently $r < 16.5$ and $r < 17.5$, respectively; but also recall the general spectroscopic *bright* limit of $m > 15$), unusually blue galaxies ($g - r < 0.2$), and moderately blue stars ($u - g < 1.1$). These medium priority spectroscopic targets are flagged as ‘ROSAT_C’ by the target selection pipeline module.

The fourth broad priority bin includes any object bright enough (but not too bright) for optical spectroscopy, that falls within the RASS circle. Objects in this class are flagged as ‘ROSAT_D’ by the target selection pipeline, and most are rather unlikely to be the proper identifications; on the other hand, it is important to allow for this group as well, lest our biases based on past studies preclude discovery space for new classes of X-ray emitters.

Among the confirmed quasars/AGN cataloged in this paper, selected for possible SDSS spectra by virtue of their interest as potential RASS identifications, the great majority were (as expected) assigned to either—or sometimes both—‘ROSAT_A’ and ‘ROSAT_B’ categories. When considering just the highest priority bin assigned: 16% were assigned ‘ROSAT_A’, 76% were assigned ‘ROSAT_B’, 3% ‘ROSAT_C’, and 5% ‘ROSAT_D’.

One subtlety of RASS/SDSS target selection is that because of the restriction noted above that optical objects within an X-ray error circle may *not* have their photometry inter-compared beforehand to pick the “best” candidate, a situation may still arise in which, for example, both a ‘ROSAT_A’ and ‘ROSAT_D’ object, well separated in the same X-ray error circle, could otherwise still both be assigned an SDSS spectroscopic fiber. In order to avoid wasting the second fiber in such a case, a trick is now imposed that effectively restricts spectroscopy in most cases to only a single SDSS candidate in each X-ray error circle: currently, only optical candidate counterparts within radius $27.5'' = 55''/2$ offset from the X-ray source are ultimately allowed for selection for spectroscopy by the target selection software module devoted specifically to RASS/SDSS. The minimum $55''$ mechanical spacing between spectroscopic fibers then ensures that only a single SDSS optical object within the X-ray error circle will actually receive a RASS/SDSS spectroscopic fiber: one in the highest priority bin offset $< 27.5''$ from the X-ray source. (If there are multiple SDSS objects of the same priority—e.g., two SDSS objects within $27.5''$ of a RASS source, both having priority class ‘ROSAT_A’—then one is chosen at random for SDSS spectroscopy).

For aid in database book-keeping, we have added an additional flag ‘ROSAT_E’, that is

now also assigned at the target selection stage to indicate an SDSS optical object of potential interest that is unsuitable for follow-up SDSS spectroscopy for any reason. For example, this flag might call attention to an SDSS object of interest outside the $27.5''$ radius offset discussed in the preceding paragraph (but within $1'$ of the RASS source position), or one too bright or too faint for SDSS spectroscopy, or one matching a RASS source with X-ray detection likelihood below 10, etc. (Note also that an SDSS object may receive more than one ROSAT target selection flag, e.g., one with ‘ROSAT_A’ and ‘ROSAT_E’ flags set might indicate a triple radio/optical/X-ray match, but one not suitable for SDSS spectra for some reason, etc.). We added the ‘ROSAT_E’ flag during the early phases of SDSS commissioning, but after early target selection was already underway; however, this late addition complicates the book-keeping on only about 10% of the objects discussed in this paper (and of course that fraction will decrease, as the sample expands).

The actual SDSS spectroscopic targeting situation is even somewhat more complex than described here (see Stoughton et al. 2002 for additional details). First, the target selection algorithms for each of the various other SDSS spectroscopic follow-up categories—quasars, galaxies, stars, serendipity objects, as well as ROSAT candidates—were under refinement in the early “commissioning” phases of SDSS. Secondly, objects that are part of the SDSS optical samples to obtain (ultimately) 10^6 spectroscopically-observed galaxies and 10^5 confirmed quasars are actually assigned their spectroscopic fibers first via a sophisticated “tiling algorithm” (Blanton et al. 2003), before *any* consideration is given to potential RASS targets. For example, an SDSS object selected as a QSO candidate by the *quasar* target selection algorithm will very likely receive a spectroscopic fiber (and e.g., even when the ROSAT algorithm flags it as ‘ROSAT_E’). Indeed, the following SDSS optical objects are nearly guaranteed to receive an SDSS spectroscopic fiber independent of X-ray emission: all galaxies to $r < 17.77$ (Petrosian magnitude), almost all SDSS PSF objects to $i < 19.1$ with colors indicative of quasars, and almost all FIRST radio sources with optical PSF-morphology to $i < 19.1$. A common benefit is that the number of distinct SDSS fibers needed specifically for RASS sources is thereby further decreased due to the large fraction—about 80%—of RASS identifications that ultimately prove to be AGN, and which were already independently targeted for spectroscopy by the SDSS *quasar* target selection algorithms (before the algorithms specifically aimed at RASS candidates ever come into play). Moreover, the *quasar* target selection algorithms are not confined to pick only objects within the $27.5''$ offset restriction imposed on RASS/SDSS targets, so additionally can sample counterparts throughout the full $1'$ X-ray error circles. Conversely though, a random galaxy targeted at high priority merely as it is part of the main SDSS galaxy redshift-survey sample, and falling by chance in a RASS error circle, may occasionally *exclude* another high-priority ROSAT target from any possibility of receiving a spectroscopic fiber. This is merely due to the $55''$ minimum fiber spacing.

The net effect is that RASS/SDSS target selection, both in general and also specifically for the objects cataloged in this paper, cannot guarantee “completeness”. However, in practice we expect the spectroscopic sample will ultimately prove to be reasonably complete at least for most classes of X-ray emitting quasars and AGN with $15 < m < 19$. Within $27.5''$ offset from the

RASS sources, such optical targets may be chosen for spectroscopy by both the quasar and the ROSAT target selection categories (and at larger positional offsets, about 80% of X-ray emitting quasars/AGN like those discussed herein may still be selected by the *quasar* target selection algorithms.)

Despite the limitations on completeness, examination of the very high-quality SDSS spectroscopy (e.g., see Figure 2) confirms that these target selection algorithms that choose odd-colored optical objects and/or radio sources within RASS error circles are highly efficient at locating X-ray emitting quasars/AGN. For example, objects selected by the ‘ROSAT_A’ and/or ‘ROSAT_B’ algorithms applied to the SDSS imaging data are confirmed to be X-ray emitting AGN conservatively more than about 75% of the time, upon examination of the follow-up SDSS spectra; in fact, approximately 85% of the spectra in these two algorithm categories are those of very likely quasars/AGN (and constitute the catalogs presented herein), but a few percent of these may be chance superpositions unrelated to the X-ray sources as we discuss in section 6, and a few percent reflect slightly more speculative spectral classifications/identifications (the Sy 2 candidates discussed near the end of section 4.2, a handful of objects among the BL Lac candidates discussed in section 4.3, and a few dozen of the objects among the large sample of NLS1s discussed in section 5.1). The efficiency of spectroscopic identifications may also be somewhat larger than quoted above for the ‘ROSAT_A’ and ‘ROSAT_B’ categories, as these same algorithms also yield: 8% other sorts of galaxies (4% are galaxies with comparatively weak/narrow or no optical emission, plus 4% radio galaxies having bland optical spectra); 3% stars, most of which are either white dwarfs or cataclysmic variables; and, 4% of the spectra that are either ambiguous or of too low S/N to definitively classify. Some fraction of these additional objects (e.g., nearly *all* of the CVs—which are already cataloged as likely X-ray sources in other SDSS papers by Szkody et al. 2002, 2003) are also plausible additional RASS IDs, but are not included, nor counted as successes, in the discussions of the current AGN paper.

4. Initial Catalog of 1200 X-ray Emitting AGN From RASS/SDSS

In this section, we present initial results towards the ultimate goal of a sample of $\sim 10^4$ well-characterized optical identifications of RASS X-ray sources. The emphasis in this installment of the RASS/SDSS catalog is on our initial set of more than 1200 X-ray emitting quasars and other sorts of AGN; as discussed below in section 6, for these AGN the identifications are secure at least in a statistical sense. The comprehensive range of Galactic and extragalactic X-ray identifications will be discussed in upcoming papers related to the SDSS Data Release 1 and beyond (e.g., Voges et al. 2003). Other ROSAT results especially from the SDSS Early Data Release (EDR), bearing on various specific X-ray emitting classes include: cataclysmic variables (Szkody et al. 2002, 2003), clusters of galaxies (Sheldon et al. 2001), EDR narrow-line Seyfert 1s (Williams, Pogge, & Mathur 2002), and EDR quasars (Schneider et al. 2002; Vignali, Brandt, & Schneider 2003a).

4.1. Quasars and Other AGN with (Predominantly) Broad Permitted Lines

In Tables 1 and 2 we present a catalog of 964 spectroscopically confirmed RASS/SDSS quasars and closely-related AGN having (predominantly) broad permitted emission lines; all have optical positions within $1'$ of RASS X-ray sources. Sample Tables 1 and 2 (listing just the first 5 entries) are included within this paper itself; the full tables are available electronically from the Journal, or upon request to the authors (contact the lead author). We include under this present category of quasars and other “broad-line” AGN all such RASS/SDSS objects whose spectra show characteristic strong optical emission lines of AGN, with broad permitted emission having velocity width in excess of 1000 km/sec FWHM. For low redshift objects in the range out to about $z < 0.4$ where MgII 2800 is not yet accessible, we rely on the $H\beta$ emission line to make this velocity-width determination; for higher-redshift AGN, we merely consider the FWHM of the broadest line observed within the SDSS spectroscopic coverage. Note that, aside from luminosity and data quality criteria, this category is defined similarly to that of the Schneider et al. (2002) EDR quasar catalog. However, we here avoid any *a priori* luminosity cuts, and so these first tables will include not only most quasars, but also most Sy 1s, many Sy 1.5s, and even many of such unusual but interesting classes as NLS1s.

Nearly all (about 98%) of these “broad-line” AGN were selected for spectroscopy by either the ROSAT or the quasar target selection algorithms (or both as discussed above) applied to the SDSS imaging database.¹⁹ This catalog reflects objects having follow-up SDSS spectroscopy parameters stored within a database accessible to the SDSS collaboration (for internal reference, we refer to this as the “Chunk 8 database”) as of early 2002; that database included information from 269 (distinctly numbered) spectroscopic plates, of which 251 are in common with spectroscopic plates included in the most recent public data release (“Data Release 1”; Abazajian et al. 2003). All objects have confirming, high-quality SDSS optical spectra; see Figure 2 for representative examples. About 20% of these objects were both already-cataloged as quasars/AGN and also had redshifts reliably established prior to SDSS, and the bulk are newly-identified as X-ray emitting AGN from combined RASS/SDSS data. Other objects are previously cataloged in Bade et al. (1998a) and related lists, but lacked secure identifications in their low-resolution grism/prism spectral data. (See also Margon et al. 2000, Voges et al. 2001, Schneider et al. 2002, Williams et al. 2002, and Vignali et al. 2003a for discussions of various subsets of the several hundred AGN identifications available earlier from the EDR.) In this paper, Table 1 catalogs mainly empirical

¹⁹As an additional check on the autonomous target selection algorithms discussed above, we also have considered *post facto* (and cataloged here as AGN where appropriate) all SDSS objects with an optical spectrum that fall within $1'$ of a RASS source, and independent of whether or not actually selected by the ROSAT target selection algorithms described in the preceding section. For this additional check we externally cross-correlated with the RASS catalogs the positions of $\sim 200,000$ optical objects having spectral information incorporated into the SDSS database as of early 2002, and examined all 3141 resulting SDSS spectra. This additional check confirms that the autonomous RASS/SDSS target selection pipeline algorithms are working as anticipated, and are not missing any substantial set of X-ray emitting AGN.

characteristics of the 964 X-ray-emitting broad-line quasar/AGN counterparts obtained from SDSS, while Table 2 provides other derived information discussed herein. In both tables, objects are ordered according to the J2000 RA of the RASS X-ray source.

In Table 1, emphasizing observed parameters, the *1st column* provides the RASS X-ray source position (J2000) using RA/Dec nomenclature. The *2nd column* similarly provides the optical position/nomenclature (J2000) of the suggested quasar/AGN counterpart as measured from SDSS data; the optical astrometry is accurate to better than $0.1''$ (Pier et al. 2003). The *3rd through 7th columns* provide optical photometry in the 5 SDSS passbands (e.g., Fukugita et al. 1996) in the *asinh* AB system (Lupton, Gunn, & Szalay 1999); as the final SDSS photometric calibrations were not completed at the time this project began, the PSF magnitudes in Table 1 are denoted with an asterisk, and the estimated calibration uncertainties are of order a few percent. The *8th column* provides the value of the SDSS imaging parameter ‘objc_type’, a commonly used and reliable SDSS measure of optical morphology (see Stoughton et al. 2002 for more details); objc_type=6 indicates stellar/unresolved optical morphology, while objc_type=3 indicates an extended/resolved (i.e., galaxy) morphology. The *9th column* provides the redshift as measured from the SDSS spectra; in most cases the quoted redshift is that provided by the SDSS spectroscopic pipeline, but we have confirmed all redshifts by an independent manual/by-eye check, and agreement in most cases (except for a handful that we have corrected in the tables based on our manual measures) was to within 0.01 in z . The remaining columns of Table 1 emphasize the X-ray data on the broad-line quasars/AGN, and are derived directly from the RASS catalogs (e.g., see Voges et al. 1999, 2000). The *10th column* provides the RASS X-ray source count rate (counts/sec) in the 0.1-2.4 keV broadband, corrected for vignetting. The *11th column* gives the RASS exposure time in seconds. The *12th and 13th columns* provide X-ray hardness ratios as measured from several X-ray bands (see Voges et al. 1999). The *14th column* is the X-ray source detection likelihood (a maximum likelihood measure of source significance). The *15th column* gives the estimated X-ray flux in the 0.1-2.4 keV band, as observed, i.e., without corrections for absorption in the Galaxy; we used the PIMMS (Portable, Interactive, Multi-Mission Simulator) software to convert RASS count rates into X-ray fluxes, assuming a power-law X-ray spectrum with energy index $\alpha_x = 1.5$ typical of (low redshift) quasars in the RASS passband (e.g., see Schartel et al. 1996).

In Table 2, we present further catalog information on the 964 broad-line RASS/SDSS AGN, but now also emphasizing derived quantities used herein. For more convenient cross reference we repeat some relevant information included within Table 1. The *1st column* and *2nd column* repeat, respectively, the RASS X-ray source and suggested optical counterpart name/position. The *3rd column* provides the extinction-corrected g -band PSF magnitude, corrected according to the reddening maps of Schlegel, Finkbeiner, & Davis (1998). The *4th column* repeats the redshift from SDSS spectroscopy. The *5th column* is the X-ray flux (units of 10^{-13} erg/s/cm²) in the 0.1-2.4 keV band, now corrected for absorption within the Galaxy, and with absorbing columns estimated from the N_H column density measures of the Stark et al. (1992) 21cm maps. The *6th, 7th, and 8th columns* give the logarithms of, respectively, inferred broadband (0.1-2.4 keV)

X-ray luminosity (units of erg/s), monochromatic UV/optical luminosity (units of erg/s/Hz) at a frequency corresponding to rest frame 2500 Å, and monochromatic soft X-ray luminosity at 2 keV; we adopt values of $H_0=70$ km/sec/Mpc, $\Omega_M = 0.3$, and $\Omega_\Lambda = 0.7$ for deriving the luminosities in Table 2. In converting from corrected broadband (X-ray 0.1–2.4 keV, and optical g -band) flux to luminosities, we again assume an X-ray power-law spectrum with energy index $\alpha_x = 1.5$, and an optical power-law with energy index $\alpha_o = 0.5$. The *9th column* lists α_{ox} , the slope of a hypothetical power law (in energy) from the UV/optical to X-ray (i.e., connecting 2500 Å and 2 keV). The *10th column* provides brief comments, e.g., noting selected objects that are radio sources, including one alternate name for objects whose spectral classification and accurate redshift were both available (in catalogs/papers incorporated into NED) prior to SDSS, noting the $\sim 1\%$ of the cases where two of our cataloged AGN fall within the same RASS error circle (latter denoted as ‘ambigID’ in the comments), etc. Again, only the initial 5 entries are included in this sample Table 2 within this paper itself; the full table is available electronically from the Journal and the lead author, as indicated above.

4.2. X-ray Emitting AGN Having Narrower Permitted Emission

In addition to the predominantly “broad-line” (FWHM>1000 km/sec) AGN discussed above in section 4.1, we also examined and approximately classified the spectra of all other extragalactic emission line objects in RASS error circles observed spectroscopically by SDSS. Primarily, this was done to ensure fuller sampling of the specific possible X-ray emitting AGN subclasses like NLS1s, Sy 1.5s, 1.8s, and 1.9s that have optically-observable broad-line regions; i.e., objects very closely related to classic quasars and Seyfert 1s, but which may be observed to have narrower permitted line components as well. In addition, we have also extended this subset to include Seyfert 2 candidates, i.e., AGN whose optical emission is nearly entirely dominated by a narrow-line region. The additional AGN cataloged in this section are exclusively at low redshift, so again it is initially the $H\beta$ line width/profile that we consult. That is, the objects discussed in this section all have $\text{FWHM}(H\beta)<1000$ km/sec based on a *naive* (and in many cases here, incorrect) line measure that assumes a single component to the line profile.

For classification as Sy 1.5 to Sy 1.8, we require the full width near the continuum level (hereafter, FWZI) of the $H\beta$ emission line to exceed 2500 km/sec. Of course measurements near the continuum are problematic near $H\beta$, especially when Fe is strong, but except for the unusual case of some NLS1s, we have also verified that the FWZI of the $H\beta$ line exceeds that of the O[III] 5007 emission in the same object by at least ~ 1000 km/sec; hence each such object has a “broad-line” component substantially wider than typical of its narrow line region. The taxonomical classifications provided in this section are mainly intended as an aid in clarifying why these objects, although similar, did not satisfy the specific criteria discussed in section 4.1 for (predominantly) “broad-line” quasars and AGN. To make the specific taxonomical subdivisions simple but more concrete, we label as Sy 1.5 those objects having *both* broad and narrow $H\beta$

components and with relatively small [OIII] $\lambda 5007$ to $H\beta$ flux ratios of $R < 3$, and label those with $R > 3$ as Sy 1.8s; see Whittle (1992) for a similar sub-classification scheme.²⁰ (The NLS1s are discussed in more detail in section 5.1).

We also select a number of low redshift objects in RASS error circles, whose SDSS optical spectra show little or no evidence for broad $H\beta$, but which do appear to have a markedly broad $H\alpha$ emission component. We refer to these (somewhat loosely) as Sy 1.9s; however, in low S/N cases, weak broad $H\beta$ may not be well-measured or even recognized, so some of these are likely to really be Sy 1.5–1.8s. To help limit confusion in these “Sy 1.9” cases between truly broad $H\alpha$ and those in which narrow $H\alpha$ is merely blended with [NII] emission, as well as complications of contaminating late-type stellar continuum/absorption features in cases with substantial host-galaxy stellar light, we very conservatively limit our Sy 1.9 candidate list here to include just those cases with very broad $H\alpha$, requiring $\text{FWZI}(H\alpha) > 6000$ km/sec.

Finally, we also extend our catalog a little to include candidate X-ray emitting Sy 2s and related AGN. Possible identifications of Sy 2s, starbursts, and other narrow emission line galaxies as X-ray emitting subclasses have been discussed in multiple papers most recently emphasizing deeper, higher spatial-resolution, and/or harder energy X-ray imaging surveys (e.g., Boyle et al. 1995, McHardy et al. 1998). However, in some cases subsequent improved follow-on optical spectroscopy has led to ultimate reclassifications (e.g., Halpern, Turner, & George 1999) into one of the categories already considered above, e.g., NLS1, Sy 1.8, Sy 1.9, etc. Nonetheless, an extension to include X-ray emitting Sy 2 candidates may be of interest for several reasons including: Type 2 AGN are sometimes invoked as significant contributors to the cosmic X-ray background, and nearby bright examples may be individually interesting if *bona fide* Sy 2s; and, even if the candidates discussed herein are not confirmed as X-ray emitting Sy 2s upon closer scrutiny, this group might still serve to encompass some unusually subtle cases of X-ray emitting Sy 1.8-1.9s, NLS1s, etc. We select candidate Sy 2s from among the remaining narrow emission line galaxies, using AGN emission line diagnostics that are founded on the oft-used Baldwin, Petersen, & Terlevich (1981; hereafter, BPT) diagrams and criteria. We employ the specific criteria of Kewley et al. (2001) based on the relative line strengths of [OIII] $\lambda 5007/H\beta$, [NII] $\lambda 6583/H\alpha$, and S[II] $\lambda 6717, 6731/H\alpha$; the Kewley et al. criteria quantify regions in the $O[III]/H\beta$ vs. $[NII]/H\alpha$ and $O[III]/H\beta$ vs. $[SII]/H\alpha$ BPT diagrams populated by AGN versus starbursts.²¹

We catalog in Tables 3 and 4 basic empirical and derived information for the additional 216 X-ray emitting AGN discussed in this section (194 with observed broad-line regions, plus 22 Sy 2 candidates). Tables 3 and 4 for these additional AGN are analogous to Tables 1 and 2, respectively, presented above in section 4.1; and again, only sample tables are included within this

²⁰We do not attempt here to sub-classify cases like Sy 1.2s, intermediate between Sy 1 and Sy 1.5.

²¹Except that we do not consider the relatively weak *OI* line in our Sy 2 classifications. See also Zakamska et al. (2003) and Kauffmann et al. (2003) who apply similar classification approaches to much larger *optical* samples of possible SDSS Type 2 AGN.

paper, with the full tables available electronically. In Table 4, the comment column may include the subclass type, and we denote some especially uncertain classifications with a question mark (e.g., ‘Sy 2?’). Figure 3 shows selected SDSS spectra from objects in this second diverse set of X-ray emitting AGN (and see section 5.1 for further details on NLS1s).

4.3. BL Lac Candidates

We have also examined our RASS/SDSS sample for BL Lac candidates, which (by the subclass definition) would, of course, not be found in the above samples of AGN with prominent emission lines. Because of their rarity (only a few % of the objects in current quasar catalogs), and unusual properties (nonthermal continua, with strong X-ray and radio emission and nearly featureless optical spectra, high polarization, marked variability, and possible “negative” evolution—e.g., Urry & Padovani 1995, Morris et al. 1991), large and well-defined samples of BL Lacs are eagerly-sought, but until recently have proven extraordinarily difficult to assemble. Their rarity demands large areal sky coverage, and yet their unusual spectral energy distributions and lack of strong spectral features often render traditional quasar/AGN optical-selection incomplete and/or inefficient for BL Lacs. Despite numerous attempts, until recently there were only a handful of homogeneous BL Lac samples of even modest-size from which to study their remarkable characteristics.

Many recent efforts (e.g., Stocke et al. 1991, Perlman et al. 1996, Laurent-Muehleisen et al. 1997, Bade et al. 1998b) to obtain well-defined BL Lac samples utilize a combination of multiwavelength information from the X-ray, optical, and radio bands to obtain high selection efficiency. Stocke et al. (1991), Perlman et al. (1996), and others noted that BL Lacs have distinctive multiwavelength flux-ratios; e.g., BL Lacs have unusually large f_x/f_{opt} ratios compared to other AGN, and nearly all those cataloged that may confidently be called BL Lacs are radio sources as well. We employ these same general approaches and criteria within our ‘ROSAT_A’ target selection algorithm (as discussed in section 3) to obtain an initial list of RASS/SDSS BL Lac candidates. (We again also consider *post-facto* all optical spectra of SDSS objects taken in the relevant RASS circles, to ensure our algorithms are not missing a significant subset.)

We find/recover 38 objects we consider as *probable* X-ray emitting RASS/SDSS BL Lacs. For all these higher confidence cases: (1) the SDSS optical object is within $1'$ of a RASS source; (2) the SDSS object is also a positional match to a radio source (e.g., conservatively taken as $< 2''$ in this initial study for matches to FIRST sources, or $< 20''$ for matches to other radio catalogs); (3) our measures from the SDSS optical spectrum reveal no strong emission ($EW < 4 \text{ \AA}$); and, (4) there is no CaII H&K break/depression evident in the SDSS optical spectrum, or any such break present must be only very weak (quantitatively, the measured ratio of the galaxy’s flux redward of any break to that blueward is required to be less than < 1.33 , e.g., see Stocke et al. 1991, Dressler & Schectman 1987). The latter criterion reflects the circumstance that X-ray selected BL Lac sometimes have weak breaks, but not entirely featureless optical spectra (due to sometimes more pronounced starlight contamination from the host galaxies); of course, many of the RASS/SDSS

BL Lacs do indeed have approximately classically featureless optical spectra, as we show below. We also find/recover as *possible* BL Lac candidates 7 additional objects that are within RASS error circles and which either: satisfy the first three criteria (X-ray/radio sources with no strong optical emission), but which just barely miss on the fourth criterion (2 objects that have CaII break flux ratios of between 1.33 and 1.40); or, have too low S/N in their SDSS optical spectra to claim the BL Lac spectral nature of criteria (3) and (4) with much confidence (3 objects); or, which show approximately featureless SDSS spectra, i.e., that satisfy criteria (1), (3), and (4), but where a close match has not been made to a radio source (2 objects).

In the 1400 deg² of sky considered here then, a total of 45 candidate optical counterparts satisfy these criteria as probable or possible BL Lacs, and basic information is provided for them in Tables 5 and 6 (which are analogous to Tables 1 and 2 for emission line AGN). Again, only the initial 5 entries are included in these sample tables; the full tables are available electronically from the Journal and the lead author. In the comment column of Table 6, we use ‘zunc’ to denote selected cases where the redshift from SDSS is highly uncertain, and the redshift is not available from (or is different in) the literature. (Of course, the quoted redshifts may also be lower limits on the actual BL Lac redshift, if the spectral absorption arises in foreground material rather than in the BL Lac host galaxy.) If a redshift is not obtained from the SDSS spectrum, nor already available in the literature, we adopt $z = 0.3$ (near the median of others in the sample) for estimating α_{ox} in Table 6; as this is essentially a ratio of luminosities, aside from precise K-corrections, the values of α_{ox} should be approximately correct in most cases. In Table 6, we denote the possible but less certain BL Lac candidates as ‘BL?’ in the comment column. Example SDSS spectra of selected BL Lac candidates are shown in Figure 4.

About half of these objects have been previously-reported in the literature as BL Lacs or BL-Lac-like objects, and some other objects are previously cataloged in Bade et al. (1998a) and related lists, but lacked secure identifications in their low-resolution grism/prism spectral data. Even among the previously-cataloged BL Lacs, SDSS provides the first high-quality published optical spectra for many objects, and new spectroscopic redshift estimates (admittedly uncertain in some cases) for 9 of the previously cataloged BL Lacs. Where redshifts were available prior to SDSS, there is also usually good agreement with our SDSS measures, and in total 2/3 of the full sample of 45 have spectroscopic redshifts estimated from SDSS spectra, and/or other slit-spectra already published in the literature.

A few of the suggested BL Lac identifications may eventually prove to be misidentifications where a radio galaxy lies within an X-ray emitting cluster or other group of galaxies (e.g., Rector, Stocke, & Perlman 1999). Others may prove to be stars upon higher S/N or resolution spectroscopic follow-up; but it is worth recalling that all but a couple are both X-ray and radio sources, and so are more likely to be BL Lacs than highly unusual X-ray/radio stars. As an additional precaution in the latter regard, we have also considered proper motion information. Collinge et al. (2003) are independently optically selecting SDSS BL Lac candidates using lack of optical emission and lack of significant proper motions (via comparison with the POSS) as their

principal criteria. None of our 45 RASS/SDSS BL Lac candidates has significant proper motion (>20 mas/yr), e.g., suggesting little contamination by nearby hot white dwarfs, etc.

Thus, it seems likely that most of the BL Lac identifications are correct (see also section 6 below). In the ultimate RASS/SDSS joint sky coverage, we may thus predict with some confidence that we will be able to quantitatively define a sample of several hundred X-ray BL Lac candidates.

5. Discussion of Other Rare Classes and Individual Objects of Interest

5.1. Narrow-line Seyfert 1s (NLS1s)

Among our RASS/SDSS AGN (including objects discussed in both sections 4.1 and 4.2), we identify from the SDSS spectra a total of 133 likely, and another 36 possible, X-ray emitting NLS1s. These objects are denoted by ‘NLS1’ (likely) or ‘NLS1?’ (possible) in the comment columns of Tables 2 and 4. Gallo et al. (2003) are investigating this interesting subclass in detail from the current RASS/SDSS samples, and Williams et al. (2002) have recently discussed about 45 of these same objects independently selected from the EDR. The reader is thus referred to those far more extensive investigations. But briefly, these objects have unusually narrow permitted lines, though in other aspects are more similar to Sy 1s than Sy 2s; in the X-ray, these objects often show strong soft X-ray excesses, and marked variability. A variety of explanations have been suggested for NLS1s, including unusually low-mass black holes, higher accretion rates relative to Eddington, nearly pole-on orientation, unusually thick broad-line regions, etc. (e.g., see recent reviews by Boller 2000 and Pogge 2000).

The 133 X-ray emitting examples we label as reasonably confident cases all have low [OIII] $\lambda 5007$ to $H\beta$ flux ratios (we very conservatively restrict confident cases to $R < 1$), $H\beta$ FWHM less than 2000 km/sec, and strong optical Fe emission—representative characteristics of the NLS1 class (e.g., Pogge 2000). The 36 less certain examples have either [OIII]/ $H\beta$ ratios of $1 < R < 3$, weaker Fe, or lower quality and therefore more ambiguous SDSS spectra, etc. Among the 1/3 of the confident cases overlapping with Williams et al. (2002), we find good ($\sim 85\%$) agreement between our spectral classifications and theirs. Representative SDSS spectra for NLS1s are shown in Figure 5.

5.2. BALQSOs

Initial ROSAT studies (Green et al. 1995), and numerous subsequent follow-on studies, have shown that BALQSOs as a class are weak emitters in soft X-rays. This deficiency at soft energies is usually interpreted as due to absorption of low energy X-rays in BAL material of surprisingly high column densities, typically inferred equivalent to $N_H \sim 10^{22-23}$ cm $^{-2}$ (e.g., Green et al. 2001 Gallagher et al. 2002). There are several *possible* BALQSOs or quasars with mini-BALs among

the RASS/SDSS X-ray identifications discussed here, but these are not yet confirmed definitively. Shown in Figures 6a and 6b are the SDSS spectra of two such possible cases.

The numbers sampled thus far are tantalizing but conservatively still somewhat too small for definitive conclusions about the paucity of BALQSOS among RASS/SDSS X-ray identifications. For example, SDSS spectral coverage yields good information on CIV BALs at redshifts above about $z > 1.7$, and our RASS/SDSS sample thus far includes about 50 such objects. If high-ionization BALQSOS comprise of order 10% of the quasar population, and if there were no bias against them in soft X-ray surveys, we would have expected to have found of order a half-dozen such BALQSOS within the current sample. Results for low-ionization BALQSOS are similar: low-ionization cases are probably present among only a few percent of the quasar population, so that once again only about a dozen might have been anticipated (even if “normal” in soft X-rays) within our current sample of about 450 RASS/SDSS quasars with $0.5 < z < 2.2$ (for which Mg II BALs might be easily identified from the SDSS spectra). Although the results for BALQSOS are thus yet not quite definitive, future expansions of the RASS/SDSS sample—ultimately encompassing $\sim 5\times$ as many objects as considered here—should allow rather stringent constraints on the incidence of BALQSOS in soft X-ray surveys.

5.3. Other Miscellaneous Interesting Subclasses/Objects

In addition to NLS1s with strong optical Fe emission discussed in section 5.1, there are another 71 objects with strong Fe emission (especially optical, but sometimes in UV), but with permitted line-widths in excess of the usual maximum of 2000 km/sec considered applicable to the NLS1 class. We denote these in Table 2 with ‘Fe’ in the comments column. Example SDSS spectra are shown in Figures 6c and 6d.

In addition, there are also a half-dozen intermediate Seyferts which might be termed Sy 1.5–1.8, but where the broad weak $H\beta$ component appears markedly asymmetric (and/or complicated with Fe emission); Figure 6e shows one such example. There are additional objects that have strong and broad MgII typical of classic quasars, but which if at slightly lower redshift might have been classified as about Sy 1.8 based on the $H\beta$ line strength/profile; Figure 6f shows an example, and one in which there appears to be both broad strong $H\alpha$ and MgII, but only rather weak broad $H\beta$.

There are many additional cases with unusual optical line profiles, including objects with very broad (~ 20000 km/sec FWZI) lines (Figure 6g), as well as other AGN with multiple-peaked line components (Figure 6h). Many of the latter objects are included in the detailed study of Strateva et al. (2003).

6. Discussion of Ensemble Properties and Reliability of Identifications

In the 1400 deg² of sky considered here, more than 1200 X-ray emitting quasars or other AGN are identified as likely RASS counterparts, each with uniform optical photometry and high-quality optical spectroscopy from SDSS. As discussed above, the SDSS optical spectra not only permit accurate redshifts, but also quantitative classification (based on widths and line-ratios) into various AGN subclasses. In this section, we return to a discussion of the ensemble properties of our sample.

The optical magnitudes (Figure 7a) for the quasars/AGN extend over the entire range accessible to routine SDSS spectroscopy of $15 < m < 21$, though the median of $g = 18.7$ is typical of past related optical identification efforts. Interestingly, even at the brightest end, there are dozens of X-ray emitting quasars/AGN brighter than 17th magnitude not cataloged prior to SDSS. The redshift distribution for the quasars is also shown in Figure 7b, and again the median redshift of $z = 0.4$ is typical of previous identification work at similar X-ray flux levels. However, our initial RASS/SDSS AGN catalog already includes 23 suggested quasar counterparts at $z > 2$, including one possible identification even for a redshift $z = 3.56$ quasar.²²

The distribution of offsets (Figure 8) between the RASS X-ray positions and the SDSS optical positions is approximately as expected if the 1200 AGN are indeed the proper identifications, at least in a statistical sense. For example, as shown in Figure 8a, 84% of the SDSS quasars/AGN fall within 30'' of the RASS X-ray positions, in approximate agreement with independent expectations about the RASS positional uncertainty distribution as a function of X-ray detection likelihood (Voges et al. 1999); the latter may be derived from Tycho stars also detected in the RASS. Figure 8b shows a slightly different representation of these positional offset data, where now the offsets have been normalized relative to the RASS positional error; the latter accounts for the dependence of the RASS positional uncertainty on the X-ray source significance, total X-ray counts detected, etc. Figure 8b also confirms that the RASS positional error estimates are reasonable ones, e.g., with more than 97% of the suggested identifications found within an offset smaller than 3 times that predicted from the RASS X-ray positional error. The small number with larger offsets (about 3% of the sample) is also consistent with the approximate expected number of random coincidences between SDSS quasars and the RASS error circles sampled, as we describe below.

We also show in Figure 9 one last related measure of the distribution of positional offsets between RASS X-ray sources and various extragalactic SDSS optical objects (having SDSS spectra). As one simple indicator of the association of various object subclasses with RASS X-ray sources, we display histograms of the distributions of the squares, r^2 , of the positional offsets

²²The $z = 4.9$ quasar SDSSp J173744.87+582829.5 mentioned in Anderson et al. (2001), that falls within (though rather far out in) a RASS error circle is *not* confirmed as an X-ray source counterpart in *Chandra* follow-up; the X-ray source has been positionally pinpointed in *Chandra* images by Vignali et al. (2003b) to fall well away (about 45'') from the high-redshift quasar.

between the SDSS optical positions and the RASS X-ray source positions; i.e., we count the fraction of objects falling within equal area annuli offset from the RASS X-ray source positions. For a chance superposition of SDSS objects within RASS error circles, these histograms would be approximately flat with r^2 . We conservatively limit consideration (in Figure 9) to objects that fall just within the $r < 27.5''$ offset discussed in section 3; all the “target selection” algorithms for selecting objects for SDSS fiber spectroscopy may work within this smaller region, while for greater offsets the ‘ROSAT’ algorithms may not select targets for SDSS spectra (and therefore could produce an artificial truncation in the distributions for larger r^2). Figure 9 shows separate r^2 histograms for quasars/AGN with predominant broad-lines discussed in section 4.1 (upper left), quasars/AGN with narrower permitted lines discussed in section 4.2 (upper right), as well as the BL Lac candidates discussed in section 4.3 (lower left); in each of these cases, the histograms for the AGN are very strongly-peaked at small r^2 values, as expected if these AGN are statistically the proper (i.e., with low contamination) X-ray source identifications.

For comparison, the lower right panel of Figure 9 shows the r^2 histograms for other normal galaxies (with weak or no emission) within $27.5''$ of RASS sources. (We have excluded error circles where we have already identified the probable X-ray counterpart as among the 1225 AGN discussed in sections 4.1-4.3, or where there is a previously known X-ray emitting cluster). Although this figure suggests the possibility of a very weak statistical correlation between some of these galaxies and RASS X-ray sources, it especially confirms that contamination by random superpositions is very high for these normal galaxy cases—contamination an order of magnitude higher than for the AGN/quasars. Although the ensemble of such more normal galaxies may well be suitable for follow-on “X-ray image stacking” or “survival analysis” statistical studies appropriate for samples with a large fraction of X-ray non-detections, they are not considered further in the current paper whose focus is on secure X-ray source identifications of AGN.²³

A related estimate of the expected number of random coincidences of quasars/AGN with RASS X-ray sources further quantifies the statistical reliability of the cataloged quasar/AGN identifications. The surface density of SDSS *optically*-selected quasars is of order $15/\text{deg}^2$, while the combined area covered by all RASS error circles considered in the 1400 deg^2 area of this initial sample is less than about 4 deg^2 . Thus, as the above positional arguments also suggest, only a small fraction ($< 5\%$) of the 1225 proposed quasar/AGN counterparts are likely to be spurious random chance positional coincidences, for which the RASS X-ray source and SDSS quasar/AGN are in fact unrelated.

²³For example, one might consider looking for hidden AGN among some brighter subset of such normal galaxies that also have small X-ray/optical positional offsets. Indeed, limiting consideration to $g < 18$ and offsets $< 27.5''$ yields an r^2 distribution for 16 bright normal galaxies that is only a little less peaked than that seen for the AGN in Figure 9. However, these 16 galaxies are sufficiently bright in the optical that only 2 have $\log(f_x/f_{opt}) > 0.1$ and therefore significantly exceed the f_x/f_{opt} range observed for other normal galaxies (e.g., Stocke et al. 1991). The exceptions are a well-studied Virgo galaxy (NGC 4636) with an extended X-ray halo (e.g., Jones et al. 2002), and a radio galaxy RX J1725.3+5255 (e.g., Bade et al. 1998a) that may also be in a group or cluster.

The distribution of the ratios of X-ray to optical flux for 1158 quasar/AGN identifications with observed broad emission line regions (we exclude the Sy 2 and BL Lac candidates, as both classes are known to have distinct flux ratios vs. broad-line AGN) is also as expected for typical X-ray emitting quasars/AGN. It has been long recognized that roughly as much energy is emitted in the X-ray as in the optical bands, as is reaffirmed by the empirical distribution (Figure 10a) of f_x/f_{opt} for the AGN considered here. In estimating the flux ratio f_x/f_{opt} , we adopt for f_x the (corrected) 0.1-2.4 keV X-ray flux (from Tables 2 and 4), and estimate the optical broadband flux in a 4000-9000 Å bandpass using the g -band PSF magnitudes (again from Tables 2 and 4) and assuming an optical power law in energy with index $\alpha_o = 0.5$. The observed distribution (Figure 10a) of f_x/f_{opt} for RASS/SDSS quasars/AGN is very similar to that found for the EMSS quasars/AGN (see Stocke et al. 1991).

Similarly, Figure 10b shows the distribution of f_x/f_{opt} ratios for the 45 RASS/SDSS BL Lac candidates discussed in section 4.3. Although distinctly different than the distribution for the quasars/AGN in Figure 10a, the BL Lac distribution we find here is very similar to that found in earlier X-ray selected BL Lac samples (e.g., again see Stocke et al. 1991). The agreement of these f_x/f_{opt} distributions with expectations for both quasar/AGN and BL Lac classes, again further confirms that the great majority of the suggested RASS/SDSS AGN identifications are in fact likely correct.

7. Discussion of An Example Multiwaveband Correlation

The large survey sample size and uniformity and quality of observational data present a variety of opportunities for follow-on detailed studies of correlations between optical and X-ray wavebands for AGN. Although this paper primarily presents the initial catalog information, we also include here one illustrative example of the sample’s potential use in studies of correlations between X-ray and optical wavebands.

As depicted in Figure 11, the 1158 X-ray emitting AGN with broad-line regions discussed in sections 4.1 and 4.2 (Sy 2 and BL Lac candidates are again excluded for reasons discussed above) also appear to show the very long-recognized non-linear correlation between optical and X-ray wavebands found in many earlier studies/samples (e.g., Avni & Tananbaum 1985). Although ours is, of course, an X-ray selected sample, the relationship we find (Figure 11a) between X-ray and optical monochromatic luminosity, $l_x \propto l_{opt}^{0.89 \pm 0.01}$, is in excellent agreement with (though with smaller formal errors than) that found in some optically-selected samples also studied via ROSAT (e.g., see Green et al. 1996; Vignali et al. 2003a). This correlation is virtually unchanged when excluding the 12% of sample objects that are radio-detected. However, the relation does appear to change when separately considering lower versus higher optical-luminosity objects; if we divide the sample in two at the median value $\log(l_{opt}) = 29.63$, we find $l_x \propto l_{opt}^{0.82 \pm 0.03}$ for the half of the objects above the median l_{opt} , and $l_x \propto l_{opt}^{0.98 \pm 0.03}$ for the half below the median (see also the discussion in the last paragraph of this section).

Similar consistent results are obtained when alternately regressing α_{ox} against optical luminosity. For the same total ensemble of 1158 quasars/AGN with observed broad-line regions, this regression yields $\alpha_{ox} \propto l_{opt}^{0.041 \pm 0.005}$, equivalent as expected to $l_x \propto l_{opt}^{0.89}$. Figure 11b depicts this latter relationship in a slightly different form. The solid line is the best fit regression relation (fit to all 1158 points), while the error bars show the mean and the standard error in the mean value of α_{ox} , as well as the mean and standard deviations in optical luminosity, when considering averages taken in various optical luminosity bins. [Note that the vertical error bars reflect the very large number of data points (typically 70-220) averaged together to estimate $\langle \alpha_{ox} \rangle$ in each bin.]

Figure 11b once again suggests the possibility of more complex dependences than assumed in our simple regression of α_{ox} versus $\log(l_{opt})$ (or in the equivalent $\log(l_x)$ versus $\log(l_{opt})$ relation discussed above). Moreover, the general sense of little dependence of α_{ox} on l_{opt} at lower l_{opt} 's, but a stronger dependence at higher l_{opt} has also been suggested by some other studies (e.g., Yuan et al. 1998a). We caution however, that a detailed study would necessarily include proper account of selection biases, dispersions in the quantities used in the regression, multiple possible parameter dependencies (e.g., on redshift and radio luminosity), and other aspects which we have neglected here. For example, disparate dispersions in optical compared with X-ray luminosities can yield apparent, but spurious, non-unity slopes in such simple correlation analyses between l_{opt} and l_x (e.g., Yuan, Siebert, & Brinkmann 1998b). Nonetheless, this illustrative example suggests that the large size, uniformity and quality of optical and X-ray data, and range of physical parameters covered by the RASS/SDSS sample are well-suited to a variety of more detailed follow-on multiwaveband correlation studies.

8. Summary

The SDSS optical and RASS X-ray surveys are well-matched to each other via a variety of fortunate circumstances, allowing efficient large-scale identification of X-ray source optical counterparts. SDSS and RASS imaging catalog data are autonomously cross-correlated, and software algorithms employed to automatically select, and assign priorities to, candidate optical counterparts for follow-on SDSS fiber spectroscopy. Application of this approach to initial SDSS data has provided homogeneous identification and RASS/SDSS flux and spectroscopic data for a large sample of X-ray emitting quasars and other kinds of AGN. The combination of SDSS multicolor selection and RASS data—and in some cases FIRST radio information—is highly (>75%) efficient for selection of X-ray emitting quasars/AGN. In an initial 1400 deg² of sky considered, more than 1200 plausible X-ray emitting quasars/AGN have been optically identified, including numerous rare cases such as 45 BL Lac candidates and more than 130 NLS1s. As this initial area represents only a fraction of the ultimate joint RASS/SDSS sky coverage, $\sim 10^4$ fully and homogeneously characterized X-ray source counterpart identifications may be anticipated to follow by completion of the SDSS survey. The already large sample will allow for a variety of more detailed studies of various AGN subclasses and individual objects of special interest, as well as for studies of ensemble correlations between optical and X-ray wavebands.

Acknowledgments: Funding for the creation and distribution of the SDSS Archive has been provided by the Alfred P. Sloan Foundation, the Participating Institutions, the National Aeronautics and Space Administration, the National Science Foundation, the U.S. Department of Energy, the Japanese Monbukagakusho, and the Max Planck Society. The SDSS Web site is <http://www.sdss.org/>. The SDSS is managed by the Astrophysical Research Consortium (ARC) for the Participating Institutions. The Participating Institutions are The University of Chicago, Fermilab, the Institute for Advanced Study, the Japan Participation Group, The Johns Hopkins University, Los Alamos National Laboratory, the Max-Planck-Institute for Astronomy (MPIA), the Max-Planck-Institute for Astrophysics (MPA), New Mexico State University, University of Pittsburgh, Princeton University, the United States Naval Observatory, and the University of Washington.

The authors thank the late Donald Baldwin of the University of Washington for his tireless contributions to the success of SDSS.

REFERENCES

- Abazajian, K. et al. 2003, AJ, in press.
- Anderson, S.F., Fan, X., Richards, G.T. et al. 2001, AJ, 122, 503
- Avni, Y., & Tananbaum, H. 1986, ApJ 305, 83
- Avni, Y., Worrall, D. M., & Morgan, W. A. 1995, ApJ, 454, 673
- Bade, N., et al. 1998a, A&AS, 127, 145
- Bade, N., et al. 1998b, A&A, 334, 459
- Baldwin, J.A., Phillips, M.M., & Terlevich, R. 1981, PASP, 93, 5
- Becker, R.H., White, R.L., & Helfand, D.J. 1995, ApJ, 450, 559
- Blanton, M.R., Lupton, R.H., Maley, F.M., Young, N., Zehavi, I., and Loveday, J. 2003, AJ, 125, 2276
- Boller, Th. 2000, New Astr Rev, 44, 387
- Boyle, B.J., McMahon, R.G., Wilkes, B.J., & Elvis, M. 1995, MNRAS, 272, 462
- Collinge, M.J. et al. 2003, in preparation
- Condon, J.J., Cotton, W. D., Greisen, E. W., et al. 1998, AJ, 115, 1693
- Dressler, A. & Schectman, S. 1987, AJ, 94, 899

- Fischer, J.-U., Hasinger, G., Schwöpe, A. D., Brunner, H., Boller, T., Trümper, J., Voges, W., & Neizvestny, S., 1998, AN, 319, 347
- Fukugita, M., Ichikawa, T., Gunn, J.E., Doi, M., Shimasaku, K., & Schneider, D.P. 1996, AJ, 111, 1748
- Gallagher, S. C. et al. 1999, ApJ, 519, 549
- Gallo, L. et al. 2003, in preparation
- Giacconi, R., Gursky, H., Paolini, F., & Rossi, B. 1962, Phys Rev Let, 9, 439
- Gioia, I. M., Maccacaro, T., Schild, R. E., Stocke, J. T., Liebert, J. W., Danziger, I. J., Kunth, D., & Lub, J. 1984, ApJ, 283, 495.
- Green, P.J., Schartel, N., Anderson, S.F., Hewett, P.C., Foltz, C.B., Brinkmann, W., Fink, H., Trümper, J., & Margon, B. 1995, ApJ, 450, 51
- Green, P.J., Aldcroft, T.L., Mathur, S., Wilkes, B.J., & Elvis, M. 2001, ApJ, 558, 109
- Gunn, J.E., Carr, M.A., Rockosi, C.M., Sekiguchi, M., et al. 1998, AJ, 116, 3040
- Halpern, J.P., Turner, T.J., George, I.M. 1999, MNRAS, 307, L47
- Hogg, D.W., Schlegel, D.J., Finkbeiner, D.P., & Gunn, J.E. 2001, AJ, 122, 2129
- Kauffmann, G., Heckman, T.M., Tremonti, C. et al. 2003, submitted to MNRAS, astro-ph/0304239
- Jones, C., Forman, W., Vikhlinin, A., Markevitch, M., David, L., Warmflash, A., Murray, S., & Nulsen, P.E.J., 2002. ApJ, 567, L115
- Kewley, L.J., Dopita, M.A., Sutherland, R.S., Heisler, C.A., & Trevena, J. 2001, ApJ, 556, 121
- Laurent-Muehleisen, S. A., Kollgaard, R. I., Ryan, P. J., Feigelson, E. D., Brinkmann, W., & Siebert, J. 1997, A&AS, 122, 235
- Lupton, R.H., Gunn, J.E., & Szalay, A. 1999, AJ, 118, 1406
- Margon, B., Chanan, G. A., & Downes, R. A., 1982, ApJ, 253, L7
- Margon, B., Anderson, S. F., Szkody, P. et al. 2000, BAAS, 32, 1183
- McHardy, I.M. et al. 1998, MNRAS, 295, 641
- Morris, S. L., Stocke, J. T., Gioia, I., Schild, R. E., Wolter, A., Maccacaro, T., & della Ceca, R. 1991, ApJ, 380, 49
- Newberg, H.J., & Yanny, B. 1997, ApJS, 113, 89

- Perlman, E. S., et al. 1996, *ApJS*, 104, 251
- Pfeffermann, E., Briel, U.G., Hippmann H., et al., 1988, *Proc. SPIE*, 733, 519
- Pier, J.R., , Munn, J.A., Hindsley, R.B., Hennessy, G.S., Kent, S.M., Lupton, R.H., and Ivezić, Z. 2003, *AJ*, 125, 1559
- Pogge, R.W. 2000, *New Astr Rev*, 44, 381
- Rector, T. A., Stocke, J. T. & Perlman, E. S. 1999, *ApJ*, 516, 145
- Richards, G.T., Fan, X., Newberg, H.J., et al. 2002, *AJ*, 123, 2945
- Schartel, N., Green, P. J., Anderson, S. F., Hewett, P. C., Foltz, C. B., Margon, B., Brinkmann, W., Fink, H., & Trümper, J., 1996, *MNRAS*, 283, 1015
- Schlegel, D.J., Finkbeiner, D.P., & Davis, M. 1998, *ApJ*, 500, 525
- Schwope, A., Hasinger, G., Lehmann, I., Schwarz, R., Brunner, H., Neizvestny, S., Urgryumov, A., Balega, Y., Trümper, J., & Voges, W., 2000, *AN*, 321, 1
- Schneider, D. P., Richards, G. T., Fan, X., et al. 2002, *AJ*, 123, 567
- Sheldon, E. S., Annis, J., Böhringer, H. et al. 2001, *ApJ*, 554, 881
- Smith, J.A., Tucker, D.L., Kent, S.M., et al. 2002, *AJ*, 123, 2121
- Stark, A. A., Gammie, C. F., Wilson, R. W., et al. 1992, *ApJS*, 79, 7
- Stocke, J. T., Morris, S. L., Gioia, I. M., Maccacaro, T., Schild, R., Wolter, A., Fleming, T. A., Henry, J., Patrick, H. J. et al. 1991, *ApJS*, 76, 813
- Stoughton, C. Lupton, R.H., Bernardi, M., et al. 2002, *AJ*, 123, 485
- Strateva, I., et al. 2003, submitted to *AJ*
- Szkody, P., Anderson, S.F., Agüeros, M.A. et al. 2002, *AJ*, 123, 430
- Szkody, P., Fraser, O., Silvestri, N., Henden, A., Anderson, S.F., et al. 2003, *AJ*, 126, in press, astro-ph/0306269
- Urry, C. M., & Padovani, P. 1995, *PASP* 107, 803
- Vignali, C., Brandt, W.N., Schneider, D.P. 2003a, *AJ*, 125, 433
- Vignali, C., Brandt, W.N., Schneider, D.P., Anderson, S.F., Fan, X., Gunn, J.E., Kaspi, S., Richards, G.T., & Strauss, M.A., 2003b, *AJ*, in press (astro-ph/0302558)
- Voges, W., et al. 1999, *A&A*, 349, 389

- Voges, W., et al. 2000, IAUC 6420
- Voges, W., Trümper, J., Boller, Th., et al. 2001, in AGN Surveys, Proc. IAU Colloq 184, eds. R.F. Green, E. Ye. Khachikian, & D.B. Sanders, (San Francisco: ASP), p. 25
- Whittle, M. 1992, ApJS, 79, 49
- Wilkes, B.J., Tananbaum, H., Worrall, D. M., Avni, Y., Oey, M. S., & Flanagan, J. 1994, ApJS, 92, 53
- Williams, R.J., Pogge, R.W., & Mathur, S. 2002, AJ, 124, 3042
- York, D.G., Adelman, J., Anderson, J.E. et al. 2000, AJ, 120, 1579
- Yuan, W., Brinkmann, W., Siebert, J., & Voges, W. 1998, A&A, 330, 108
- Yuan, W., Sibert, J., & Brinkmann, W. 1998b, A&A, 334, 498
- Zakamska, N.L., Strauss, M.A., Krolick, J.H. et al. 2003, submitted to AJ
- Zickgraf, F.-J., Krautter, J., Appenzeller, I., Thiering, I., Voges, W., Mujica, R., Pakull, M. W., Serrano, A., & Chavarria, C. 1998, AN, 319, 42
- Zickgraf, F.-J., Engels, D., Hagen, H.-J., Reimers, D., & Voges, W. 2003, A&A, in press, astro-ph/0305535.

Table 1: Observed Parameters of Broad-Line RASS/SDSS AGN^a

RASS X-ray source RXS J (1)	SDSS optical counterpart SDSS J (2)	u^* (3)	g^* (4)	r^* (5)	i^* (6)	z^* (7)	opt morph (8)	red-shift (9)	X-ray count rate (10)	X exp tim (11)	X HR1 (12)	X HR2 (13)	X like (14)	$f_x \times 10^{13}$ (15)
000011.9+000223	000011.96+000225.2	17.83	17.58	17.69	17.65	17.66	6	0.479	0.0219	364	-0.01	-1.00	9	2.21
000250.8+000824	000251.60+000800.5	19.98	18.95	18.11	17.64	17.48	3	0.107	0.0410	388	-0.32	0.09	9	4.10
000611.9-010648	000608.04-010700.8	18.95	18.54	18.44	18.43	18.55	6	0.948	0.0243	394	-0.25	-0.66	8	2.49
000709.8+005328	000710.01+005329.0	17.18	16.87	16.64	16.69	16.05	6	0.316	0.1045	405	0.07	0.04	62	10.12
000813.3-005752	000813.22-005753.3	18.97	18.29	17.66	17.08	16.89	3	0.139	0.0508	394	-0.02	0.02	27	5.14

^a[The complete version of this table is in the electronic edition of the Journal. The printed edition contains only a sample.]

Table 2: Derived Parameters of Broad-Line RASS/SDSS AGN^a

RASS X-ray source RXS J (1)	SDSS optical counterpart SDSS J (2)	g_o^* (3)	red-shift (4)	$f_x^* \times 10^{13}$ (5)	$\log(L_x)$ (6)	$\log(l_{opt})$ 2500Å (7)	$\log(l_x)$ 2 keV (8)	α_{ox} (9)	comment (10)
000011.9+000223	000011.96+000225.2	17.46	0.479	5.43	44.76	30.29	26.22	1.56	LBQS-2357-0014
000250.8+000824	000251.60+000800.5	18.83	0.107	10.03	43.49	28.33	24.95	1.30	...
000611.9-010648	000608.04-010700.8	18.40	0.948	6.21	45.60	30.58	27.06	1.35	radio
000709.8+005328	000710.01+005329.0	16.75	0.316	24.18	44.95	30.17	26.42	1.44	radio, LBQS-0004+0036
000813.3-005752	000813.22-005753.3	18.17	0.139	12.70	43.84	28.84	25.31	1.36	...

^a[The complete version of this table is in the electronic edition of the Journal. The printed edition contains only a sample.]

Table 3: Observed Parameters of RASS/SDSS AGN Having Narrower Permitted Emission^a

RASS X-ray source RXS J (1)	SDSS optical counterpart SDSS J (2)	u^* (3)	g^* (4)	r^* (5)	i^* (6)	z^* (7)	opt morph (8)	red-shift (9)	X-ray count rate (10)	X exp tim (11)	X HR1 (12)	X HR2 (13)	X like (14)	$f_x \times 10^{13}$ (15)
002847.7+145142	002848.77+145216.3	19.66	18.88	18.44	17.98	17.71	3	0.089	0.0247	422	0.13	-0.69	14	2.80
003238.2-010056	003238.20-010035.2	18.90	18.25	17.84	17.41	17.22	3	0.092	0.0688	625	-0.10	0.46	33	6.50
003846.3+003430	003843.06+003451.7	19.82	18.43	17.95	17.67	17.32	3	0.043	0.0641	303	-0.39	0.77	18	5.38
004055.2+000039	004052.14+000057.2	18.37	18.20	18.04	18.11	17.88	6	0.405	0.0232	296	-1.00	0.00	8	1.97
004532.6-005807	004533.46-005808.8	18.78	18.56	18.32	17.97	18.04	6	0.138	0.0512	329	-1.00	0.00	14	4.88

^a[The complete version of this table is in the electronic edition of the Journal. The printed edition contains only a sample.]

Table 4: Derived Parameters of RASS/SDSS AGN Having Narrower Permitted Emission^a

RASS X-ray source	SDSS optical counterpart	g_o^*	red-shift	$f_x^c \times 10^{13}$	$\log(L_x)$	$\log(l_{opt})$ 2500Å	$\log(l_x)$ 2 keV	α_{ox}	comment
RXS J (1)	SDSS J (2)	(3)	(4)	(5)	(6)	(7)	(8)	(9)	(10)
002847.7+145142	002848.77+145216.3	18.59	0.089	7.57	43.19	28.26	24.66	1.38	radio,Sy1.5
003238.2-010056	003238.20-010035.2	18.17	0.092	15.24	43.53	28.46	24.99	1.33	Sy1.5
003846.3+003430	003843.06+003451.7	18.36	0.043	11.64	42.71	27.70	24.17	1.36	Sy2?
004055.2+000039	004052.14+000057.2	18.09	0.405	4.30	44.47	29.88	25.93	1.51	NLS1
004532.6-005807	004533.46-005808.8	18.49	0.138	11.54	43.79	28.70	25.26	1.32	...

^a[The complete version of this table is in the electronic edition of the Journal. The printed edition contains only a sample.]

Table 5: Observed Parameters of RASS/SDSS BL Lac Candidates^a

RASS X-ray source	SDSS optical counterpart	u^*	g^*	r^*	i^*	z^*	opt morph	red-shift	X-ray count rate	X exp tim	X HR1	X HR2	X like	$f_x \times 10^{13}$
RXS J (1)	SDSS J (2)	(3)	(4)	(5)	(6)	(7)	(8)	(9)	(10)	(11)	(12)	(13)	(14)	(15)
003514.9+151513	003514.72+151504.1	17.32	16.93	16.58	16.28	16.04	6	...	0.2358	359	0.35	0.25	235	27.08
020106.3+003400	020106.17+003400.2	19.35	19.06	18.43	18.14	17.83	3	0.298	0.3390	400	0.07	0.04	312	31.21
023812.9-092441	023813.67-092431.4	20.82	20.26	19.64	19.21	18.84	3	0.740	0.0345	224	0.72	0.42	17	3.32
030433.0-005409	030433.95-005404.6	19.15	18.86	18.50	18.15	17.90	6	0.513	0.0559	201	0.57	0.80	21	7.22
075436.4+391103	075437.07+391047.7	18.92	17.92	17.23	16.80	16.53	3	0.096	0.0344	422	0.06	-0.68	18	3.96

^a[The complete version of this table is in the electronic edition of the Journal. The printed edition contains only a sample.]

Table 6: Derived Parameters of RASS/SDSS BL Lac Candidates^a

RASS X-ray source	SDSS optical counterpart	g_o^*	red-shift	$f_x^c \times 10^{13}$	$\log(L_x)$	$\log(l_{opt})$ 2500Å	$\log(l_x)$ 2 keV	α_{ox}	comment
RXS J (1)	SDSS J (2)	(3)	(4)	(5)	(6)	(7)	(8)	(9)	(10)
003514.9+151513	003514.72+151504.1	16.66	...	74.47	1.27	RBS-0082
020106.3+003400	020106.17+003400.2	18.97	0.298	71.93	45.37	29.23	26.83	0.92	MS-0158.5+0019
023812.9-092441	023813.67-092431.4	20.16	0.740	7.88	45.41	29.63	26.87	1.06	RX-J0238.2-0924,zunc
030433.0-005409	030433.95-005404.6	18.56	0.513	23.62	45.47	29.92	26.93	1.15	FBQS-J0304-0054,zunc
075436.4+391103	075437.07+391047.7	17.74	0.096	10.91	43.42	28.67	24.89	1.45	RX-J0754.6+3911

^a[The complete version of this table is in the electronic edition of the Journal. The printed edition contains only a sample.]

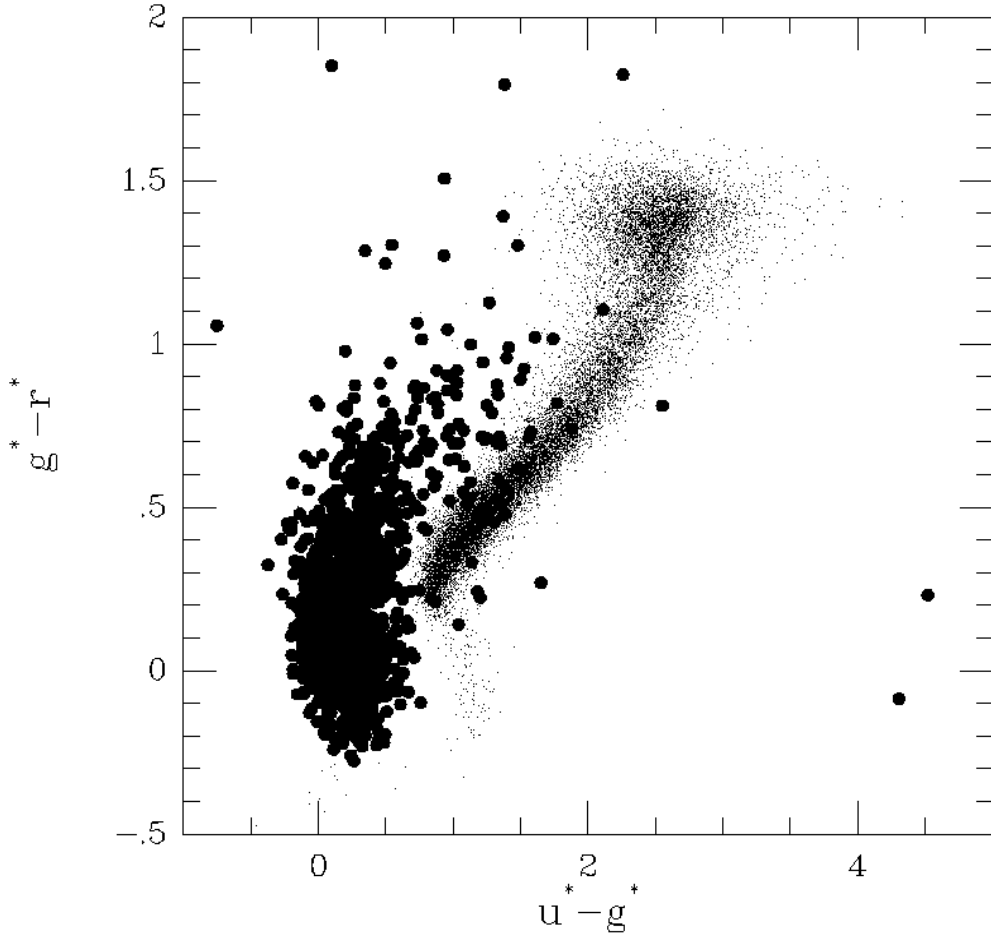


Fig. 1.— Odd colored SDSS optical objects (as well as coincidences with FIRST radio sources) and positionally coincident with RASS X-ray positions are given high priority for SDSS spectroscopic follow-up. The SDSS colors of 1225 spectroscopically-confirmed quasars and other X-ray emitting AGN in this initial sample are overplotted (large solid circles) for comparison on the locus of 10,000 anonymous SDSS stellar objects (small points). Note the clean color separation of the large majority of the confirmed quasar/AGN identifications. [For simplicity of display, three very red in $u - g$ objects (formally with PSF colors $u^* - g^* > 5$) are not shown. These objects are extremely faint in u , so their precise $u - g$ colors are uncertain.]

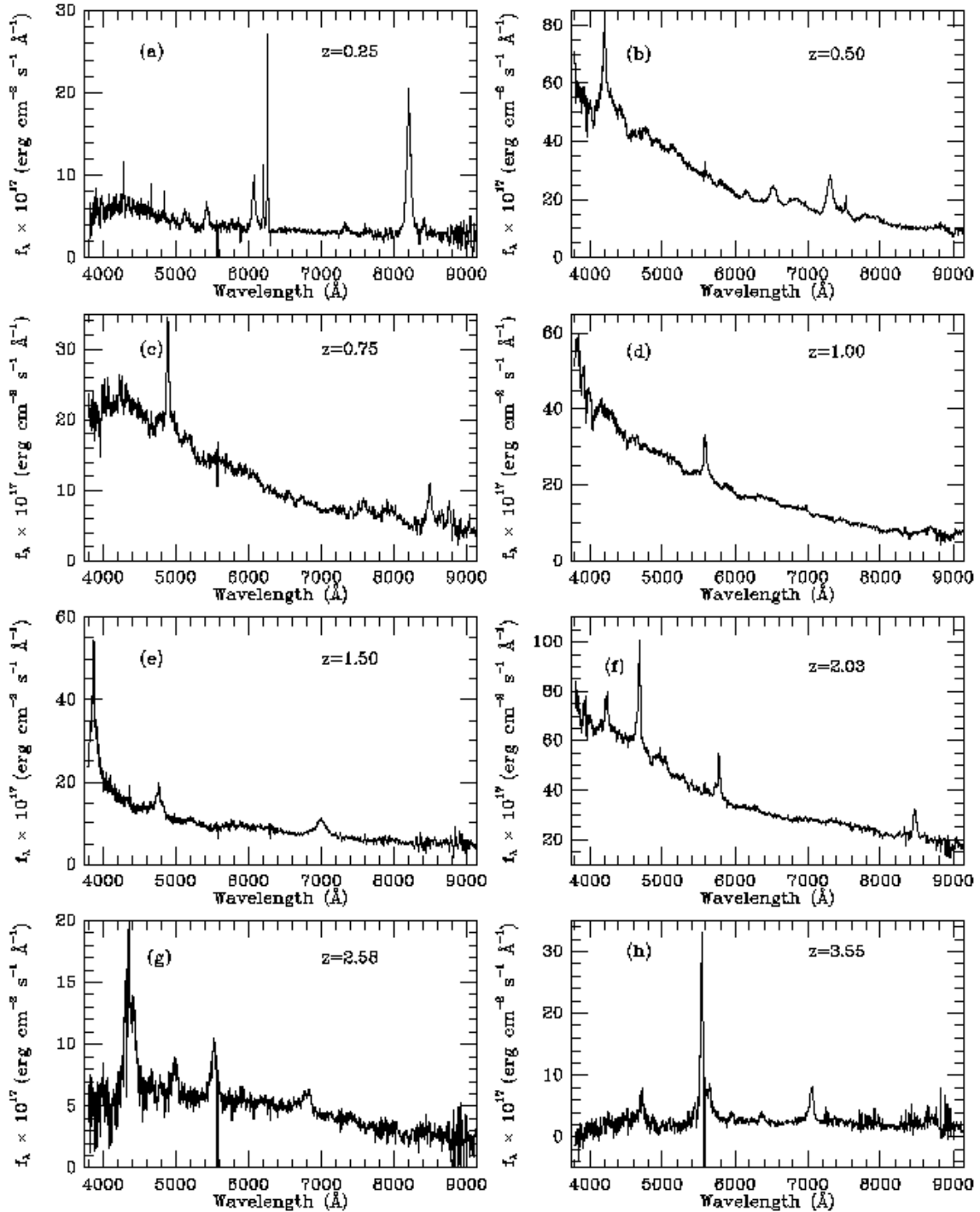


Fig. 2.— Example SDSS optical spectra for confirmed RASS/SDSS X-ray emitting quasars/AGN with (mainly) broad permitted emission, as discussed in section 4.1. Shown are spectra for typical objects covering a range of redshift from 0.25 to 3.5. All 964 such objects cataloged/discussed in section 4.1 have similar high-quality SDSS spectroscopy. (a) SDSS J233024.73+011602.3; (b) SDSS J234440.03–003231.6; (c) SDSS J103245.16+644154.2; (d) SDSS J170035.42+632522.6; (e) SDSS J172424.36+571531.0; (f) SDSS J150837.11+604955.8; (g) SDSS J155104.23+521637.7; (h) SDSS J125227.28+001001.9.

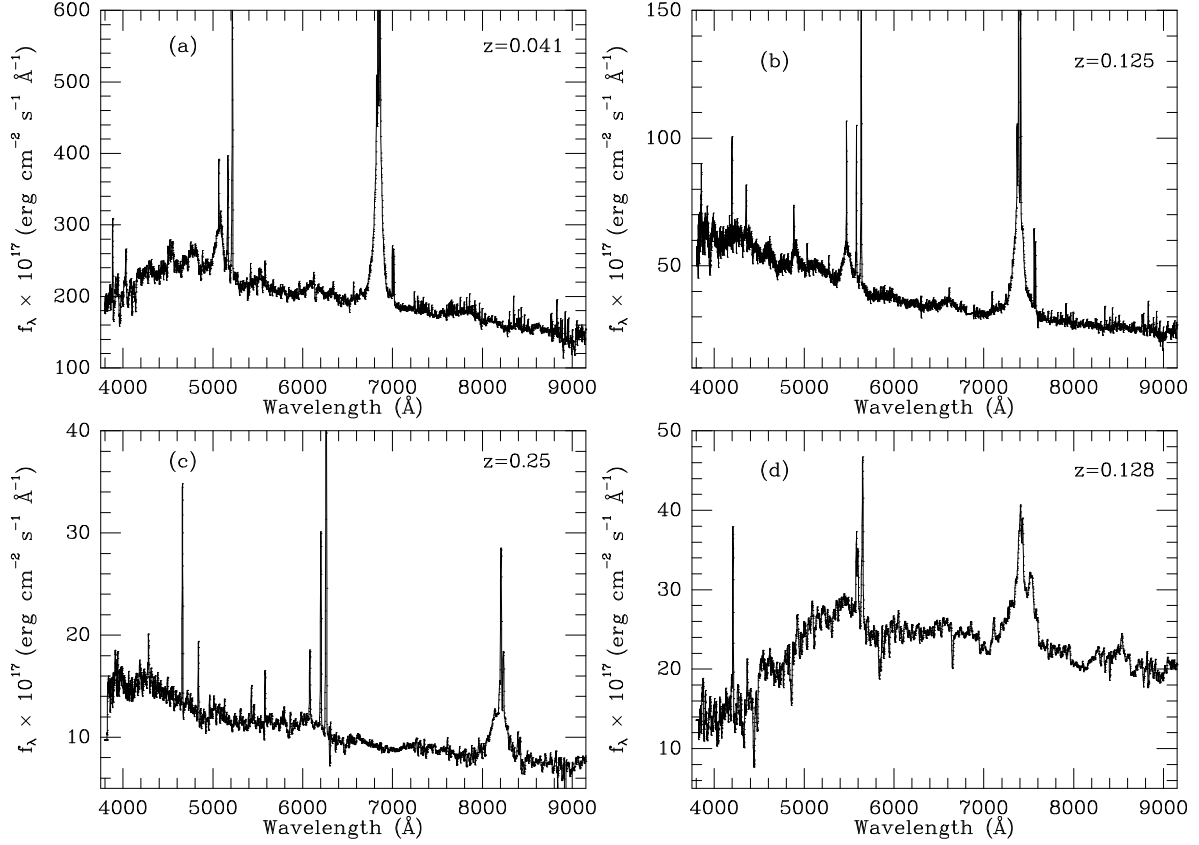


Fig. 3.— Example SDSS optical spectra for confirmed RASS/SDSS X-ray emitting quasars/AGN with both broad and narrower permitted emission components, chosen from the 216 objects cataloged/discussed in section 4.2. Shown are selected spectra for intermediate Seyfert types between Sy 1.5 and 1.9. (a) SDSS J101912.57+635802.7; (b) SDSS J112841.60+633551.3; (c) SDSS J130550.51–012331.6; (d) SDSS J082133.60+470237.2.

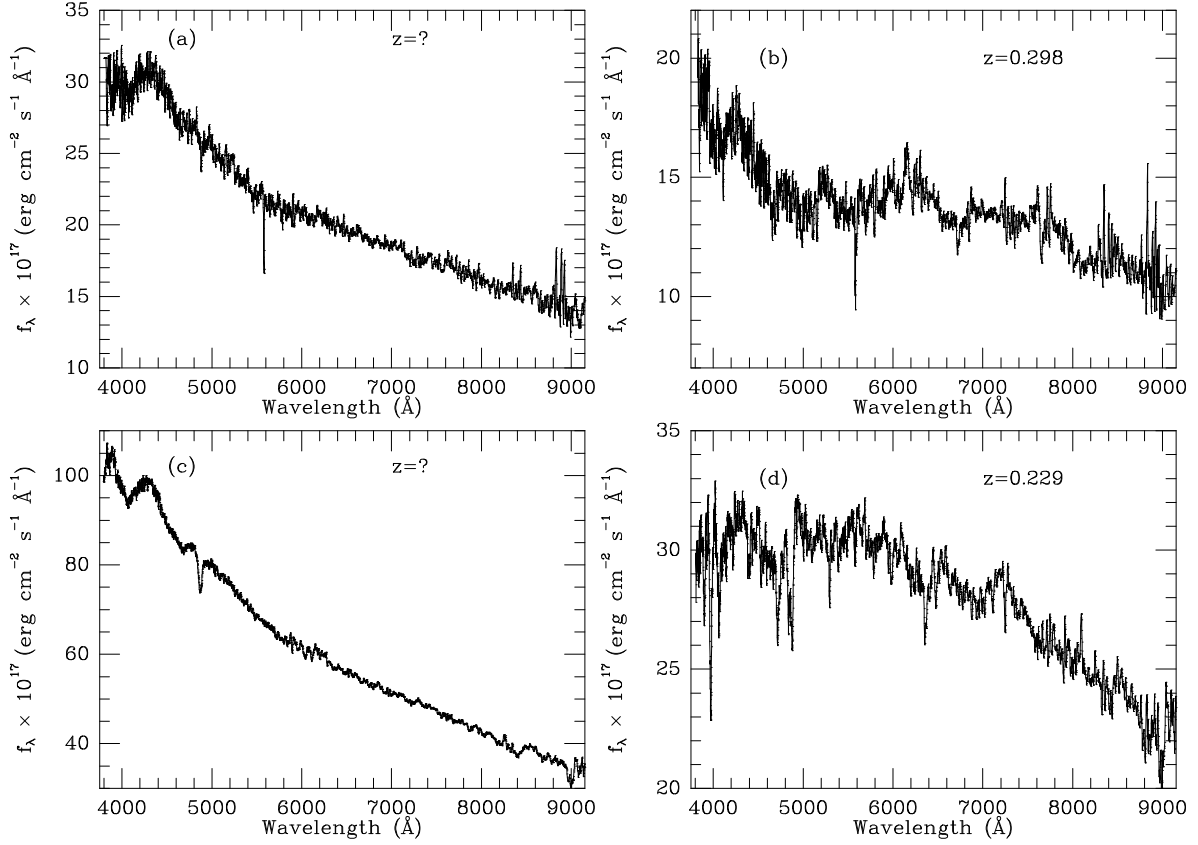


Fig. 4.— Example SDSS optical spectra of objects included in the RASS/SDSS sample of X-ray emitting BL Lacs and candidates; see text for discussion of selection. A total of 45 such candidates are presented in this initial RASS/SDSS catalog. (The apparent broad feature near 4300 Å is due to a systematic error in fluxing of the spectra). (a) SDSS J131106.47+003510.0; (b) SDSS J020106.17+003400.2; (c) SDSS J003514.72+15^h1504.1; (d) SDSS J094542.23+575747.7.

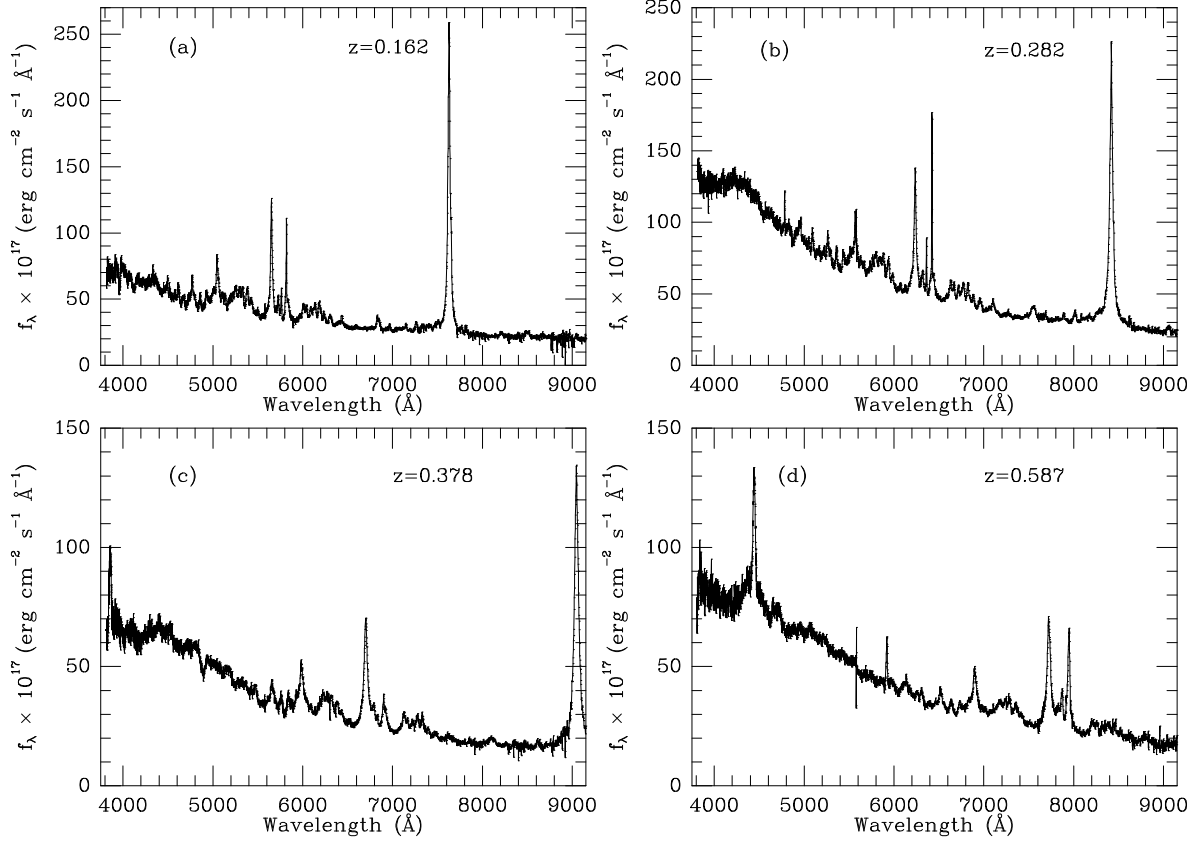


Fig. 5.— Example SDSS optical spectra for RASS/SDSS X-ray emitting NLS1s. There are 133 such confident NLS1s (and another 36 possible ones) in this initial RASS/SDSS sample. (a) SDSS J090137.99+532051.1; (b) SDSS J125100.45+660326.7; (c) SDSS J024250.85–075914.3; (d) SDSS J134948.39–010621.8.

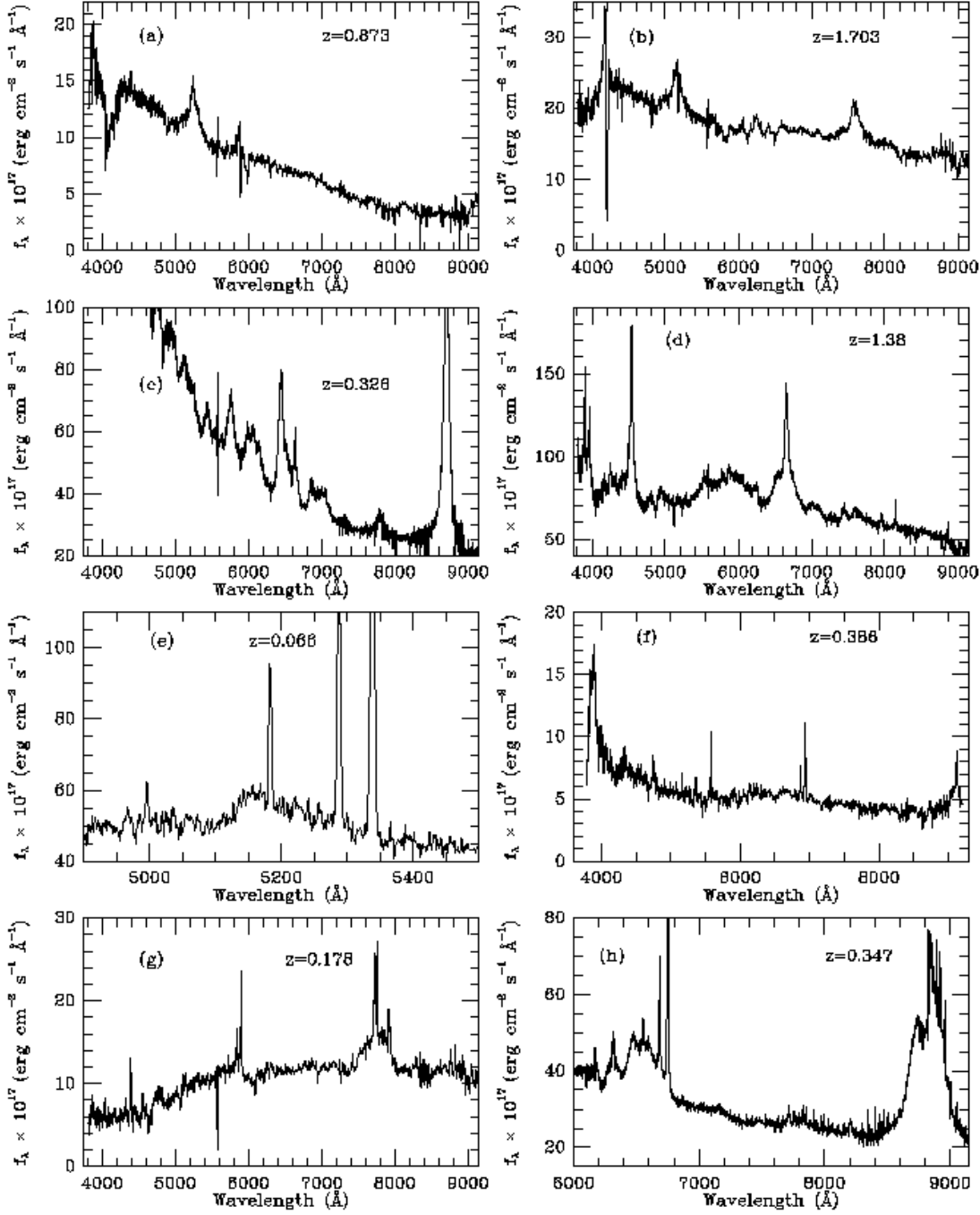


Fig. 6.— Selected other X-ray emitting AGN with unusual optical SDSS spectra. (a) SDSS J171216.28+660211.7 and (b) SDSS J150935.97+574300.5 are examples of *possible* X-ray emitting quasars with BALs or mini-BALs, though certainly not yet confirmed definitively. (c) SDSS J134251.60–005345.2 and (d) SDSS J091301.01+525928.9 are examples of strong Fe quasars, with permitted line widths in excess of those usually associated with NLS1s. (e) SDSS J172533.07+571645.5 is an example AGN with an asymmetric $H\beta$ line profile. (f) SDSS J113615.08–002314.3 is an AGN with broad weak $H\beta$ characteristic of Sy 1.8, but which has both strong and broad $H\alpha$ and $MgII$. (g) SDSS J155350.44+562230.8 is an example object with very wide line profiles of order 20000 km/sec. (h) SDSS J075407.95+431610.5 is an example of an X-ray emitting AGN in the sample with highly unusual multiple-peaked emission lines profiles.

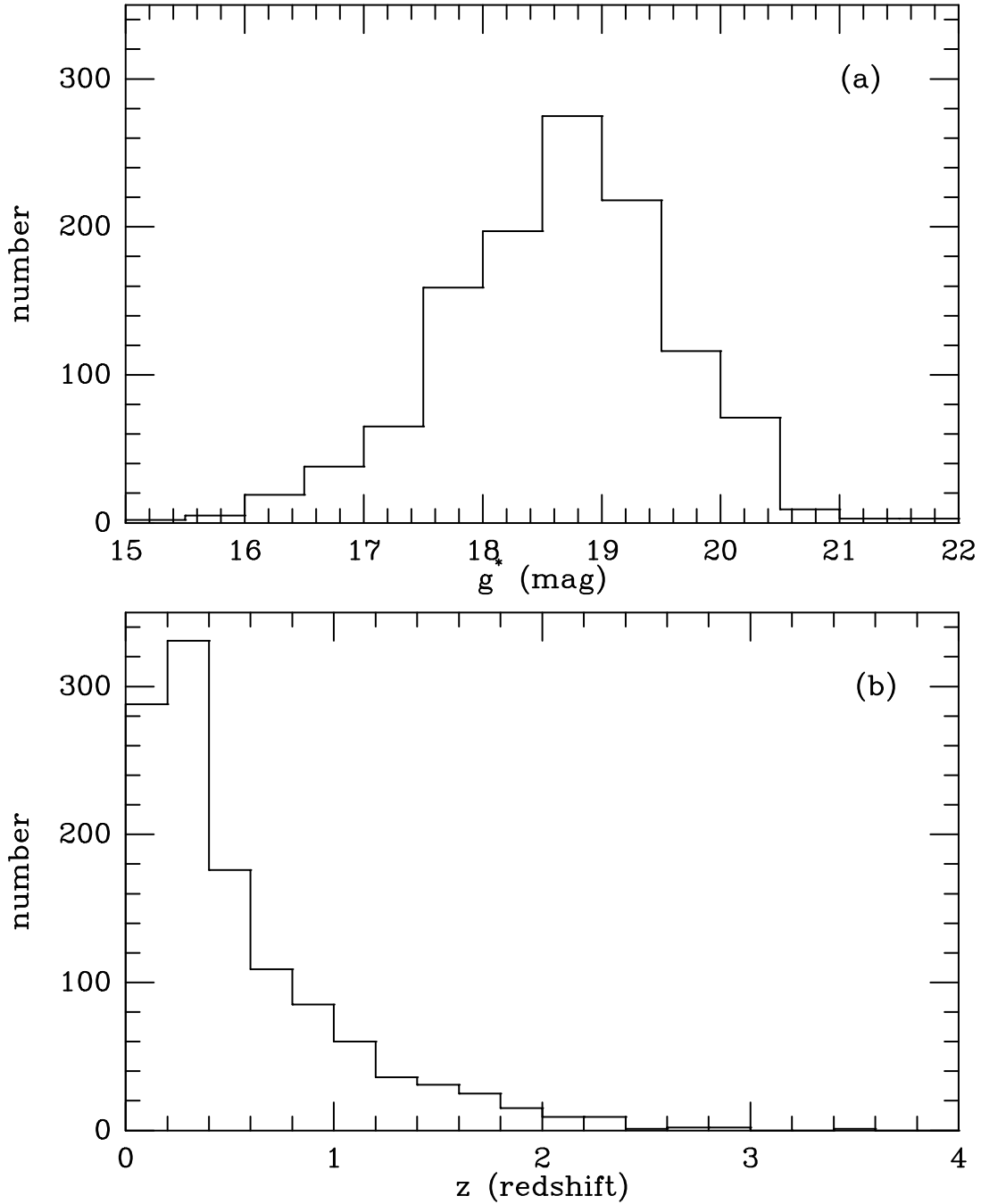


Fig. 7.— The distributions of (a) SDSS g^* -band magnitudes, and (b) redshifts, for 1180 optical counterparts of RASS/SDSS X-ray emitting AGN (BL Lac candidates excluded here). Redshifts are obtained from the high-quality follow-up SDSS optical spectroscopy. The median magnitude and redshift are typical of similar identification surveys having comparable X-ray depths. However, the large sample size permits inclusion of a significant number of higher redshift objects as well.

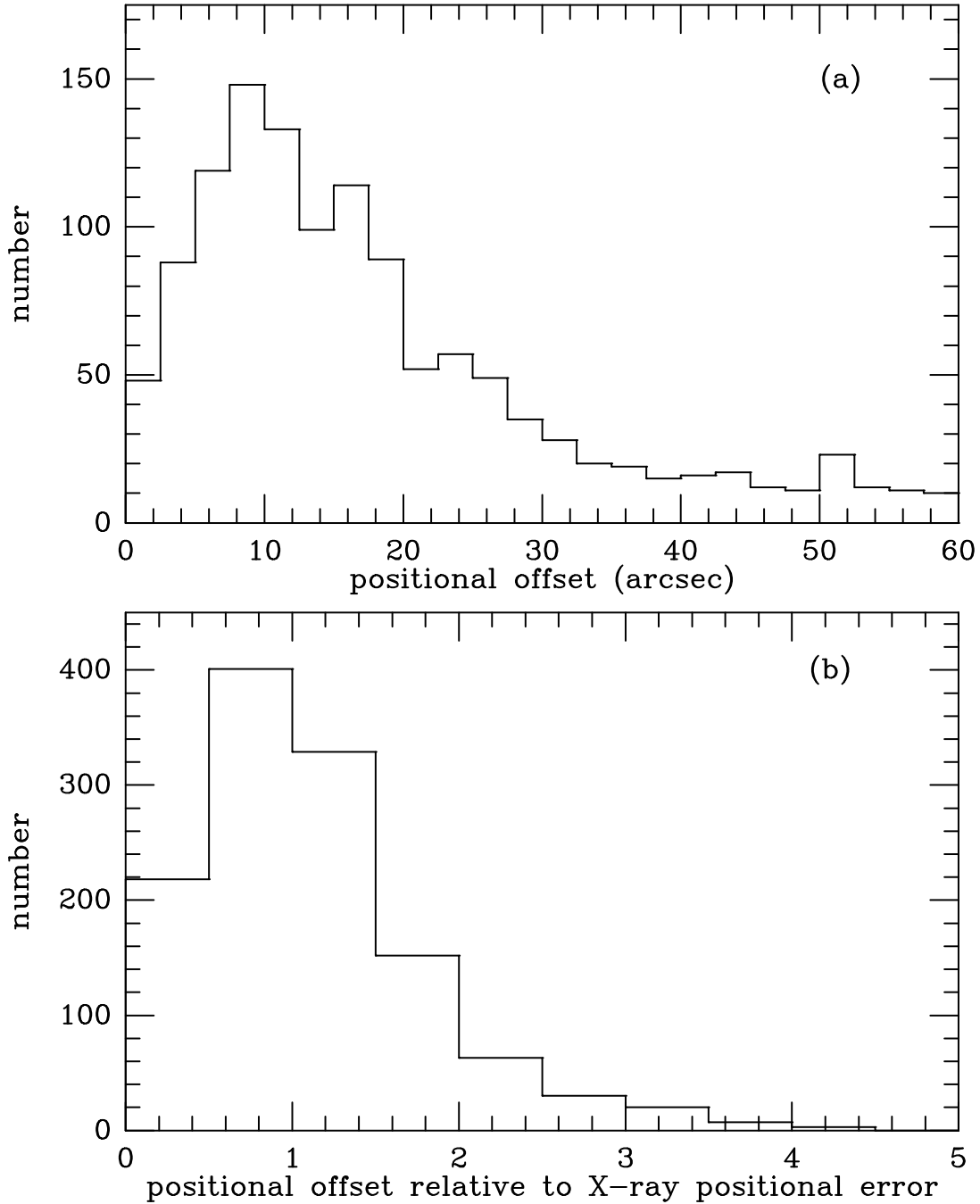


Fig. 8.— The distribution of positional differences between the SDSS optical positions of the 1225 quasar/AGN/BL Lac suggested identifications are approximately as expected if these are (statistically) the proper identifications. (a) The positional offsets in arcseconds are approximately as expected for the RASS positional accuracy, accounting for the range of X-ray detection likelihoods included. (b) The distribution of relative positional differences between the SDSS optical and RASS X-ray positions of the quasar/AGN/BL Lac identifications, in this case normalized to the expected RASS X-ray source positional error. (For ease of display, 2 objects with relative offsets >5 are excluded from this plot).

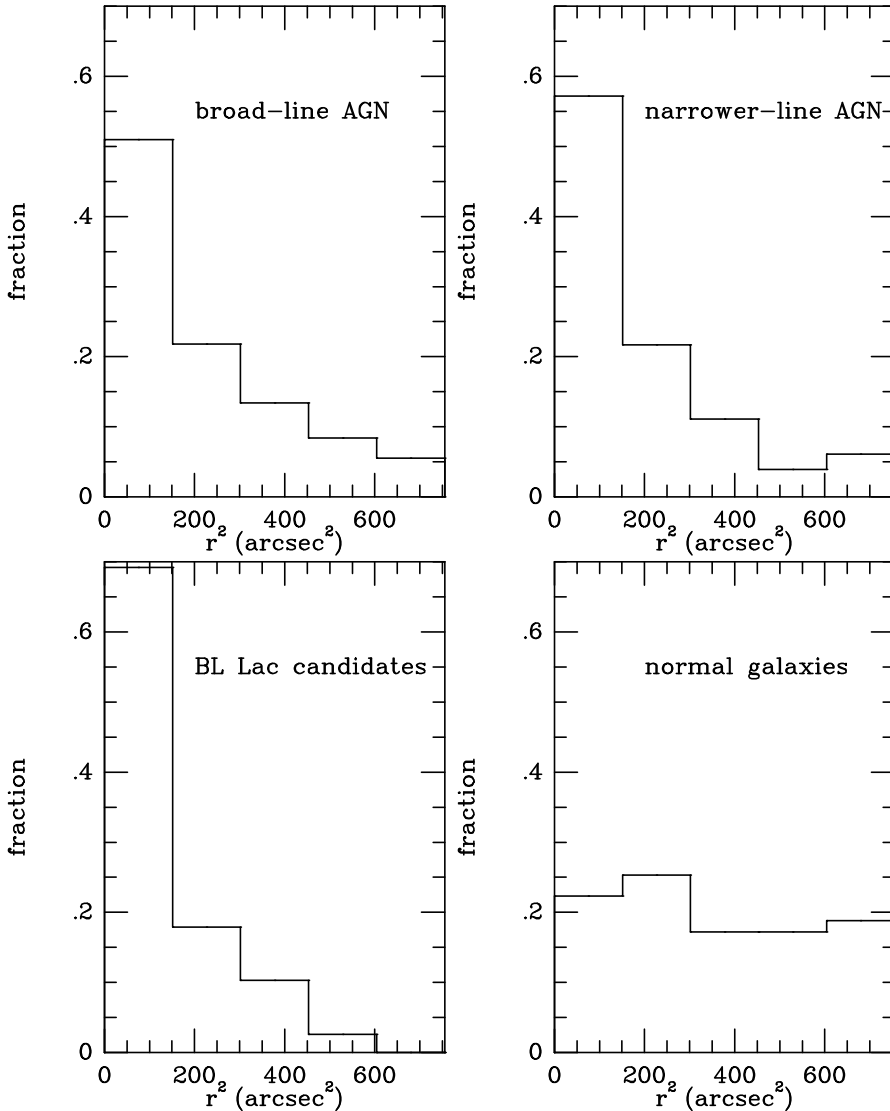


Fig. 9.— Another measure of the distribution of positional offsets between RASS X-ray sources and various extragalactic SDSS optical objects (having SDSS spectra). Plotted are histograms of the distributions of the squares, r^2 , of the positional offsets between the SDSS optical positions and the RASS X-ray source positions; we count the fraction of objects falling within equal area annuli offset from the RASS X-ray source positions. (We conservatively limit consideration to objects within $r < 27.5''$ where all relevant algorithms for SDSS spectroscopy may select targets, as discussed in section 6). Separate r^2 histograms are shown for quasars/AGN with predominant broad-lines discussed in section 4.1 (upper left), quasars/AGN with narrower permitted lines discussed in section 4.2 (upper right), as well as BL Lac candidates discussed in section 4.3 (lower left); in each of these cases, the histograms for the AGN are very strongly-peaked at small r^2 values, as expected if these AGN are statistically the proper (i.e., with low contamination) X-ray source identifications. For comparison, the lower right panel shows the histogram for normal SDSS galaxies (which, as anticipated, shows at most only a very weak statistical correlation with RASS X-ray sources).

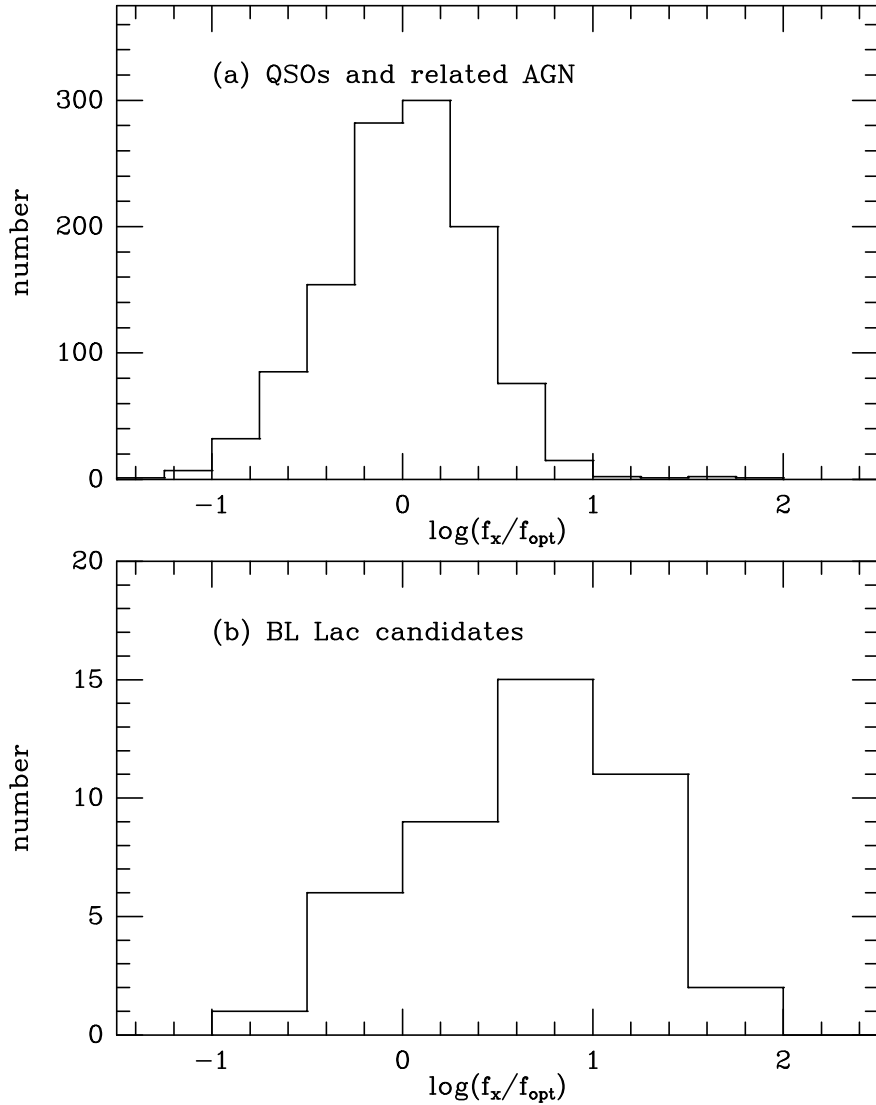


Fig. 10.— (a) The distribution of f_x/f_{opt} for the 1158 suggested quasar/AGN identifications having observed broad emission line regions (Sy 2 candidates are excluded) discussed in sections 4.1 and 4.2. As expected if these are the proper identifications, typical quasars/AGN are found to emit approximately as much energy in the X-ray as in the optical band. (b) The distribution of f_x/f_{opt} for the RASS/SDSS BL Lac candidate identifications discussed in section 4.3. The distribution is similar to that found in other X-ray selected BL Lac surveys (though markedly different than that of the emission-line quasars/AGN shown Figure 9a).

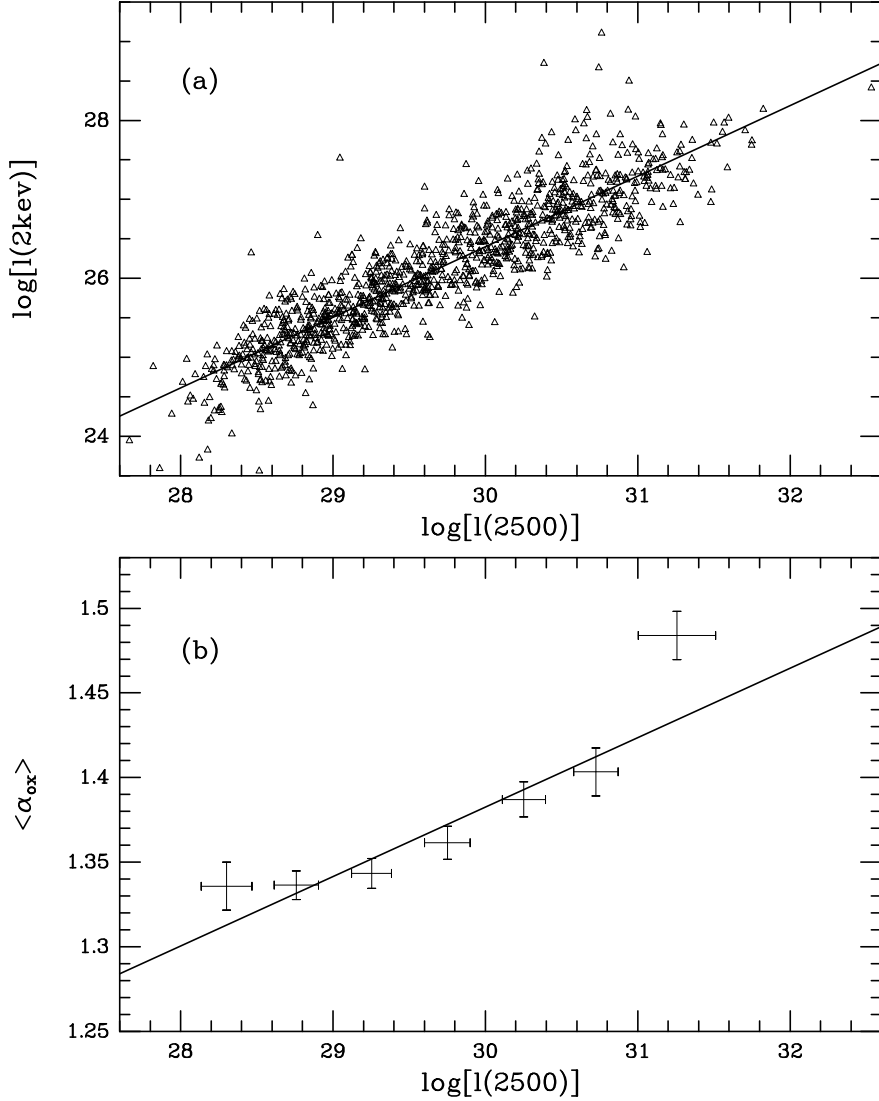


Fig. 11.— The long-recognized non-linear relationship between X-ray and optical wavebands (logarithms of monochromatic luminosities in cgs units at 2 keV and 2500Å are shown) is also seen here in our large X-ray selected sample of 1158 quasars/AGN (with broad emission line regions; Sy 2 and BL Lac candidates are excluded). (a) The solid line is a least-squares fit to the $l_{2\text{keV}}$ versus l_{2500} data, with slope 0.89 ± 0.01 . (b) Similar consistent results are obtained when alternately regressing α_{ox} against optical luminosity, and in this case linear regression yields $\alpha_{ox} \propto l_{opt}^{0.041 \pm 0.005}$, equivalent as expected to $l_x \propto l_{opt}^{0.89}$. The solid line is the best fit regression relation (fit to all 1158 points), while the error bars show the mean and the standard error in the mean value of $\langle \alpha_{ox} \rangle$, as well as the mean and standard deviations in optical luminosity, when considering averages taken in various optical luminosity bins (typically with 70 to 220 points per bin). There is an indication of a possibly more complex relation than assumed in the simple regression model.